North American Journal of Economics and Finance 73 (2024) 102152

Contents lists available at ScienceDirect

North American Journal of Economics and Finance

journal homepage: www.elsevier.com/locate/najef

Addressing the financial impact of natural disasters in the era of climate change

Michele Bufalo [a], Claudia Ceci [b], Giuseppe Orlando [a,c,*]

[a] Università degli Studi di Bari Aldo Moro - Department of Economics and Finance, Via C. Rosalba 53, Bari, Italy
[b] Università degli Studi di Roma "La Sapienza" - Department of Methods and Models for Economics, Territory and Finance, Via del Castro Laurenziano 9, Roma, I-00185, Italy
[c] HSE University, Department of Economics, 16 Soyuza Pechatnikov Street, St Petersburg, Russia

ARTICLE INFO

JEL classification:
C53
C52
G22

Keywords:
Forecasting
Natural disasters
Two-factor square-root model
Generalized Pareto distribution
Model validation

ABSTRACT

The objective of our study is to predict the financial losses that may result from natural disasters, along with their level of volatility, over a period of 1 to 15 years. Volatility can lead to significant fluctuations in Profit and Loss (P&L) for companies that are affected by unexpected events. To achieve this goal, we created a novel two-factor square-root model that allows us to establish a correlation between the frequency of occurrences and volatility, using correlated Brownian motions. Moreover, we utilized a Generalized Pareto Distribution (GPD) to estimate the maximum potential loss in terms of Value at Risk (VaR) for each specific type of natural disaster. To ensure the reliability of our predictions, we compared our results to those of four reference models and conducted a backtesting analysis. This approach is particularly suitable for insurance companies seeking to maintain stable reserves, but it can also be adapted for any other type of business that is vulnerable to extreme events and aims to safeguard a consistent cash flow for their stakeholders.

1. Introduction

Natural catastrophe modeling emerged in the late 1980s, and gained greater prominence following major events such as Hurricane Andrew in 1992 and the Northridge earthquake in 1994. These disasters highlighted the need for companies to more effectively analyze, underwrite, and price the risks associated with natural catastrophes. However, with the ongoing effects of global warming, the frequency and severity of certain climate-related events (such as floods, droughts, and storms) have exceeded the predictions of some catastrophe models. This has highlighted the limitations of traditional modeling approaches, and has necessitated the development of new techniques that can more accurately capture the potential losses from natural disasters.

The concern regarding climate change and premiums stems from the fact that, while premiums can be renegotiated annually, the estimation of reserves and actual losses is subject to uncertainties. The delay in assessing actual losses, influenced by legal and operational factors, contributes to an increase in initial losses over time. Actuarial techniques such as the chain-ladder or development are employed in loss reserving for property and casualty insurance. These techniques aim to estimate incurred but not reported claims and project ultimate loss amounts, addressing the unknown nature of actual losses, which follows a pattern known as a loss development pattern. Previously, estimates for natural catastrophe losses were based on long-term trends. However, with the advent of record-breaking hurricane seasons and predictions of increased storm activity, modelers began to incorporate near-term projections of loss into their models. This resulted in the development of models that could forecast losses up to five years in

* Corresponding author at: Università degli Studi di Bari Aldo Moro - Department of Economics and Finance, Via C. Rosalba 53, Bari, Italy.
E-mail addresses: michele.bufalo@uniba.it (M. Bufalo), claudia.ceci@uniroma1.it (C. Ceci), giuseppe.orlando@uniba.it (G. Orlando).

https://doi.org/10.1016/j.najef.2024.102152
Received 5 June 2023; Received in revised form 10 January 2024; Accepted 26 March 2024
Available online 25 April 2024

the future. Despite these advances, in some cases, the predictions generated by these models were not sufficient. As a result, new methods were developed to forecast the potential severity of the next major insured loss caused by natural catastrophes, as outlined by Hsieh (2004). This is the approach we plan to take in our research.

Traditional techniques used to model the cost of natural disasters for insurance purposes are based on geographically located assets (houses, infrastructure, activities, population density, etc.) on damage estimates that are reflected in economic losses for the insurer, type of risks (landslides, eruptions, floods, earthquakes, etc.); and adaptation measures (improved building codes, seawalls, etc.). However, this poses a great strain in terms of data requirement in terms of depth, breadth, and quality (e.g. Morton & Levy, 2011, Lythe, Shah, & Grossi, 2008 Mitchell-Wallace, Jones, Hillier, & Foote, 2017). Therefore, is not uncommon that rough approximations and strong assumptions are taken (see Calder, Couper, Lo, & Aspen, 2012).

Econometric analysis might be preferred over traditional techniques for modeling natural disaster costs in insurance due to its efficiency with reduced data requirements. Traditional methods heavily depend on detailed data about geographically located assets, risk types, and adaptation measures, leading to challenges in data depth and quality. These challenges often result in the use of rough approximations and strong assumptions, compromising model accuracy. Time series analysis offers a more streamlined approach, avoiding the data-intensive demands of traditional methods. This shift is motivated by the need for more effective modeling, given the persistent data issues and compromises associated with traditional approaches. The proposed approach would benefit insurance companies by streamlining risk modeling with reduced data requirements. Data analytics firms could conduct quicker and more cost-effective predictive modeling for natural disasters. Insurtech startups would gain innovative solutions for assessing disaster risks with fewer data demands. Government agencies might improve data processing efficiency for faster decision-making during and after disasters. Reinsurance companies might enhance risk assessment accuracy, supporting risk-sharing agreements with reduced data needs. Companies in vulnerable industries could benefit from more accessible and cost-effective risk assessments, enabling better contingency planning.

In this work, we propose a novel approach based on econometric analysis and on a stochastic model specifically designed to use a given time series of losses. The goal is not only to predict the impact of natural catastrophes (NaCat) but also their volatility. This model is suitable for NatCat since the distributions of losses are not Gaussian. In fact, in the presence of such distributions, very sophisticated models are sometimes superseded by simpler models, such as autoregressive or moving averages. In addition, regarding losses that could jeopardize an insurance company, we estimate the maximum expected loss according to the General Pareto Distribution (GPD). This estimate represents the value at risk (VaR) and is called VaRGPD. The accuracy of our results and the validity of the model are tested using Kupec (POF), Christofferson (CC) and TUFF/TBFI tests.

Furthermore, as pointed out by Anggraeni, Supian, Sukono, and Halim (2022), the application of extreme value theory (EVT) in Catastrophe Bond Pricing Models (CBPM) has uncovered deficiencies. These encompass challenges related to the application of generalized extreme value (GEV), potentially eliminating other extreme data within a period, intricacies in the trigger model, limitations associated with ARIMA allowing negative values, and the inefficacy of CIR due to its assumption of constant volatility. In response, this study addresses these gaps by employing a Generalized Pareto Distribution (GPD) to estimate the maximum potential loss, specifically in terms of Value at Risk (VaR), for each type of natural disaster. These insights underscore the significance of the proposed approach in addressing these issues and mitigating moral hazard to investors (Götze & Gürtler, 2020; Kiohos & Paspati, 2021) as sponsors face the burden of disaster losses when nearing the trigger specified to eliminate the law pliers. In such circumstances, investors may be deterred from purchasing the bonds. Hence, the market demands an earthquake catastrophe bond pricing model that is both accurate and transparent (Gürtler, Hibbeln, & Winkelvos, 2016).

To start off, we forecast the financial losses caused by some natural catastrophes as well as their volatility from short-term (1 year) to the long-term horizon (up to 15 years). In particular, we want to predict the expected value of the above-mentioned quantities which are of high importance, since it is their great variability and non-Gaussian behavior that makes any sophisticated model fallacious to the point that simple models, such as autoregressive or moving average, are more successful. Here we propose a new two-factor model with correlated stochastic volatility. This novel approach is not without its challenges, as it requires significant effort to implement and does not have readily available closed-form solutions. However, based on our model, we are able to derive an upper bound that follows a Pareto distribution and serves as a Value at Risk (VaR) estimate for backtesting purposes. This is a valuable contribution to the literature and provides an innovative tool for risk management in various industries. Being able to forecast the interaction between losses and volatility is very important for stabilizing the P&L. The proposed methodology is on the edge between banking and insurance. It has been expressly designed for insurers and reinsurers but applies as well to banks and other companies when exposed to dramatic changes in a given line of business (LOB) due to unexpected events.

As detailed in the next section, there are many stochastic models able to describe persistent jumps and high levels of volatility. Due to the high variability previously illustrated, we decided to adopt a two-factor model. Hence, in this work, we intend to show that our model is not only able to predict the average losses and their volatility but, also, can calculate a proper upper bound. The latter, in our framework, follows a Pareto distribution and represents our Value at Risk (VaR).

This paper is organized as follows. The next Section resumes the existing literature and gives an account of the reasons we have selected the suggested model. Section 3 is about materials, methods and techniques. In there, we start by describing the data source which is by the explanation of the proposed model. Backtesting analysis for model validation concludes the Section. Numerical results are illustrated in Section 4. Section 5 briefly explains the relevance in terms of premia calculation. Finally, Section 6 contains the conclusions and the Appendix contains graphical and statistical evidence of the validity of the proposed model.

2. Literature review and model selection

Natural disasters are complex and dynamic systems that can have catastrophic impacts on both the environment and human populations. The frequency and severity of these events are on the rise due to climate change and the expanding human population. These events are characterized by nonlinearity, high intermittency and low correlation, as noted by Jin, Cheng, and Wei (2008). This means that predicting the occurrence and severity of natural disasters is a challenging task, and requires sophisticated modeling techniques that can capture the complex interactions between the various factors at play. Typical tools for time series analysis are not of easy application because of discontinuity and different cycles mutually nested (Jin et al., 2008). For instance, a large set of models and tests are not applicable because they are based on Gaussian behavior. The same applies to nonlinear techniques such as ARIMA that rely on assumptions such as "stationarity, invertibility and independence of residuals" (Povinelli, 2000). More successful applications have ARCH/GARCH models because, on long-term horizons, they display weak persistency as "the time correlation disappears and a simple uncorrelated Itô process is recovered" (Carbone, Castelli, & Stanley, 2004). The squared form of the lagged shocks, however, disables the ability to deal with asymmetric volatility due to different effects that positive or negative perturbations may have (Zivot, 2009).

A different kind of model, but explicitly designed for earthquakes, is based on the Utsu (1970) framework in which a combination of a strong main shock and after-shocks is considered to assess the total damage (see for example Cai, Wan, and Ozel (2020)).

Point processes such as the Hawkes process are widespread in finance as they are able of modeling temporal events characterized by self-exciting properties (for a survey see Bacry, Mastromatteo, & Muzy, 2015 and Hawkes, 2018). They have been used for modeling order-book events, risk contagion modeling, optimal execution strategies, etc. In insurance, they can be employed for modeling earthquake swarms (Ogata, 1988) or mortality risk (Cox, Lin, & Pedersen, 2010). Multivariate Hawkes processes (Embrechts, Liniger, & Lin, 2011) are expressly designed to model multiple correlated sequences, where the occurrence of an event in a sequence may influence the occurrence of new events in another sequence. However, those processes may either fail in capturing the mutual influence between processes or may become computational prohibitive (Eichler, Dahlhaus, & Dueck, 2017; Hall & Willett, 2016; Shang & Sun, 2019). For this reason, in our quest for jointly modeling expected losses and volatility for any kind of natural disaster, we decided to not pursue this pathway.

Other traditional approaches based on geographically located assets and adaptation measures, are subject to data issues and require strong compromise (see Morton & Levy, 2011, Lythe et al., 2008 Mitchell-Wallace et al., 2017). For example, Calder et al. (2012) mention that there "may also be systemic data issue: the data for the region may not be granular or detailed enough for the component models to use the appropriate vulnerability or financial parameters, leading to potentially systemic over- or underestimation of losses. Moreover, the phenomenon of demand surge – where building costs increase due to high demand for reconstruction – would be exacerbated by multiple events from the same region. If this is deemed necessary, the most conservative way would be to assume full correlation of the SUPercentiles from events from the same peril and region".

As just mentioned, there is a wide range of models available in financial literature. As we need to model levels, volatilities and their interdependencies, we exclude unifactorial models such as those developed to deal with regime changes and cluster volatility (see Orlando, Mininni, & Bufalo, 2018, 2019a, 2019b, 2019c, Orlando & Bufalo, 2021, 2023) or based on time-varying skew Brownian motion (Ascione, Bufalo, & Orlando, 2024). In addition, as there is a trade-off between the increased benefit of having a large number of state variables and issues caused by estimations, overfitting and so on, we limit ourselves to the class of two-factor models. On those models literature is abundant (Rouah, 2013), (Tsuchiya, 2019), (Ewald, Zhang, & Zong, 2019).

The Heston model 1993, for example, may suit well because it describes the evolution of an asset jointly with its volatility. However, as Heston himself noted, an increase in volatility can capture the kurtosis of spot returns but not the skewness. Therefore, "in order to capture the skewness, it is crucial to also include the properly specified correlation between the volatility and the spot exchange rate of returns" (Ahlip, Park, & Prodan, 2017). As in our time series, kurtosis is much higher than skewness (see Table 2) this shortfall is crucial.

The so-called two-factor Gaussian models were introduced by Hull and White (1994) and then extended by Brigo and Mercurio with the G2++ model 2006. They start by defining a time-homogeneous two-factor short-term rate model to describe the dynamics of interest rates. They then add a deterministic shift function to the model to match the initial term structure of interest rates. However, "the obtained results are rather clumsy and not intuitive, which means that special care has to be taken for their correct numerical implementation" (Acar & Natcheva-Acar, 2009).

Another class of two-factor models is the one introduced by Longstaff and Schwartz (1992), which belongs to the class of stochastic mean and stochastic volatility models. Within the proposed framework, Longstaff and Schwartz approached interest rate volatility and term structure modeling by linking up yields to volatility. This framework performs better than the GARCH model (Bollerslev, 1986) because the addition of the volatility as a second state variable allows more freedom in modeling humps, troughs, and interconnectedness between levels and volatility. Empirical evidence found that the short rate exhibits volatility clusters which can be well approximated by stochastic volatility (Faff & Treepongkaruna, 2013). More recently, Christoffersen, Heston, and Jacobs (2009) modeled levels by a stochastic high mean reversion factor and correlations between returns and variance by a second factor with lower mean reversion. Similarly, Recchioni and Sun (2016) modeled asset price dynamics by a two-factor model where the first factor represents stochastic interest rates and the second one stochastic volatility. On pricing and risk in natural gas markets, Kohrs, Mühlichen, Auer, and Schuhmacher (2019) proposed a multidimensional variant of the Longstaff–Schwartz model for deriving options' properties under realistic price dynamics.

Other models, commonly used for studying the tail behavior of distribution, are based on the extreme value theory (EVT). Within the EVT framework, we consider the generalized Pareto distribution (GPD) introduced by Pickands III (1975). A classical reference

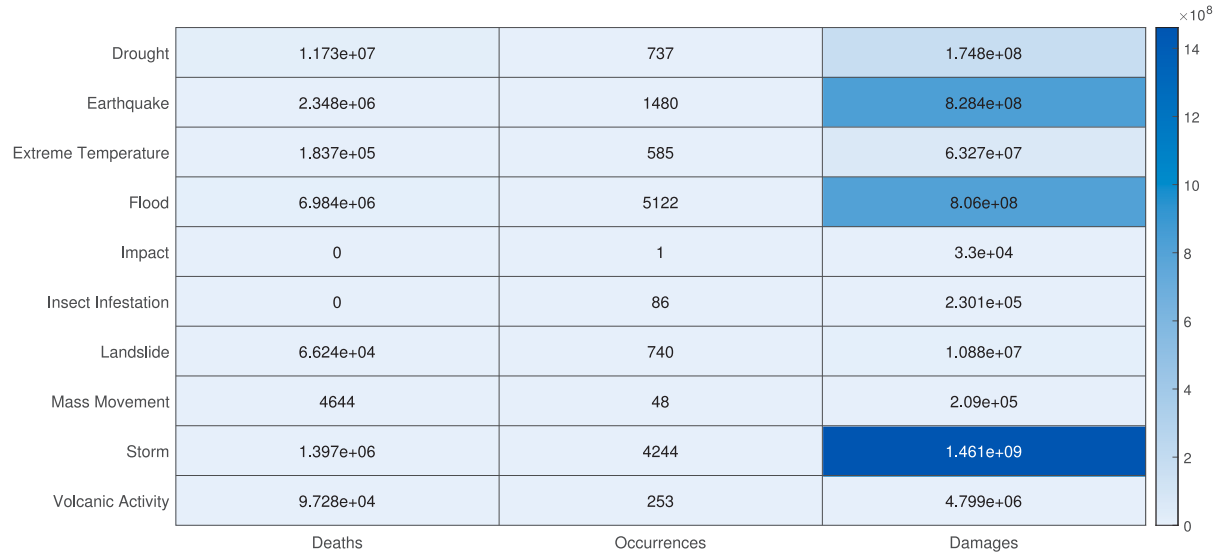

Fig. 1. Sum of deaths, occurrences and total damages (US$) of natural disasters (1900–2020).

is Coles, Bawa, Trenner, and Dorazio (2001) who introduces the theoretical framework of extreme value models and the statistical inferential techniques. GPD has applications in a number of fields, including epidemiology (Chen, Lei, Zhang, & Peng, 2015), non-life insurance (Hanafy et al., 2020), environmental extreme events (Chavas, Yonekura, Karamperidou, Cavanaugh, & Serafin, 2013; Martins, Liska, Beijo, de Menezes, & Cirillo, 2020; Orlando & Bufalo, 2022), etc. For this reason, we include it between the baseline models against which we intend to run our analysis.

The last class of models we consider as a baseline is the generalized linear model (GLM) (Nelder & Wedderburn, 1972) which allows for response variables to have error distribution models other than a normal distribution. GLM has extensive applications in insurance. For example claim sizes, frequencies and occurrences of claims do not have normal outcomes. Furthermore, the link between outcomes and risk drivers is multiplicative rather than additive (De Jong & Heller, 2008). Thus the distribution of the response is chosen from the exponential family so that the response can be heteroskedastic.

In this work, in a quite different context, we draw inspiration from the above-mentioned literature when dealing with natural disasters.

3. Materials, methods and techniques

This Section is partitioned as follows. After mentioning the dataset used for numerical results in Section 3.1, we introduce our two-factor square-root model to describe the dynamics of log-losses and their volatility in Section 3.2. Further, two baseline models for comparison and benchmarking are considered in Section 3.3. The numerical simulation and the parameter calibration of the proposed model are explained in Section 3.4. Expected value predictions of log losses and their volatility are obtained by providing, via a Generalized Pareto Distribution (GPD), a maximum threshold estimate of log losses in terms of Value at Risk (VaR). Next, measures of forecasting accuracy are defined in Section 3.5, and, finally, the most popular backtests used by financial institutions are considered in Section 3.6 to validate our model based on VaR exceedances.

3.1. Dataset

Our dataset is sourced from the Emergency Events Database (EM-DAT) hosted at the Centre for Research on the Epidemiology of Disasters (CRED). The EM-DAT database encompasses the "world's most comprehensive data on the occurrence and effects of more than 23,000 technological and natural disasters from 1900 to the present day" (CRED, 2020) worldwide. The data frequency is on an annual basis.

For our convenience, we have chosen to concentrate on the losses (adjusted for inflation) attributed to five natural disasters with a higher impact, namely earthquake, storm, flood, drought, and extreme temperature, as categorized by the data source. Fig. 1 depicts the sum of deaths, occurrences, and total damages (US$) of natural disasters from 1900 to 2020 as recorded in EM-DAT.

Table 1
Maximum of the percentage change of C_t and x_t, i.e., $C_t/C_{t-1} - 1$ and $x_t/x_{t-1} - 1$, respectively, due to natural disaster (annual data from 1900 to 2020).

	Maximum of percentage change				
	Earthquake	Storm	Flood	Drought	Ext. Temp.
Perc. change of C_t $(\cdot 10^4)$	1.97%	0.04%	1.01%	0.03%	0.26%
Perc. change of x_t	3.65%	12.56	22.25%	23.25%	9.72%

Table 2
Four indices of log-losses empirical distribution (annual data from 1900 to 2020).

	Earthquake	Storm	Flood	Drought	Ext. Temp.
Mean	11.50	12.07	11.30	9.08	4.88
Std. Dev.	3.38	5.03	7.01	7.80	5.15
Skewness	−0.92	−0.78	−0.49	−0.07	0.81
Kurtosis	3.80	2.57	1.61	1.13	2.23

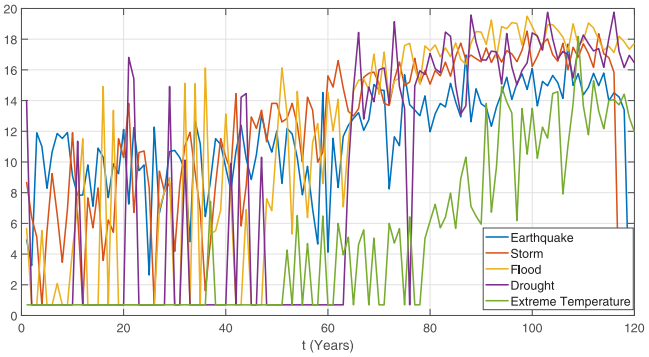

Fig. 2. Log-losses due to natural disasters (annual data from 1900 to 2020).

3.1.1. Description of data

Regarding losses, to begin with, we denote by C_t the cumulative amount of the losses at time t, i.e.,

$$C_t = \sum_{h=1}^{t} L_h,$$

where L_h denotes the single loss at the time h. To reduce the variability of the losses time series we compute the logarithmic return defined as

$$x_t = \ln\left(\frac{C_t}{C_{t-1}}\right). \tag{1}$$

For the sake of notation, we call the log-returns of the amount of the losses as "log-losses".

Natural catastrophes (often abbreviated as NatCat) encompass property policies such as earthquake and landslide failure, primary and excess storm and flood insurance, etc. Table 1 shows the magnitude of the (percentage) change of C_t and x_t, respectively, over five natural disasters with higher impact (the dataset is described in Section 3.1). Note that, in the case of C_t, volatilities are of the order of magnitude between 10^3 and 10^4 which makes complicates any forecasting attempt. Therefore, due to the high variability of time series and as commonly done in finance, we are going to consider the log-losses x_t only.

Further, in Fig. 2 the log returns are plotted for the five chosen natural disasters, whereas Table 2 reports the sample mean and standard deviation of x_t as well as the skewness and kurtosis of their empirical distribution. Note that the logarithms shown in Fig. 2 are always positive as the amount of losses C_t increases over time. Obviously, this is different from the Gaussian distribution.

Finally, Fig. 3 illustrates the shifts in the five selected perils, indicating potential changes attributable to climate change—specifically, highlighting those cases where increases in severity are expected compared to changes in frequency.

3.1.2. Hurst exponent

As explained in the introduction, the first step in our approach is to understand the dynamics of natural disasters in terms of persistence and randomness. Persistence refers to the tendency of a time series to follow a trend, while randomness refers to the degree to which the series deviates from a trend. To quantify this, we use the Hurst exponent (H_e) (Hurst, 1956), which ranges from 0 to 1. A low H_e value suggests that the series is anti-persistent and anti-correlated, an H_e value around 0.5 indicates randomness, and high values suggest persistent and correlated dynamics.

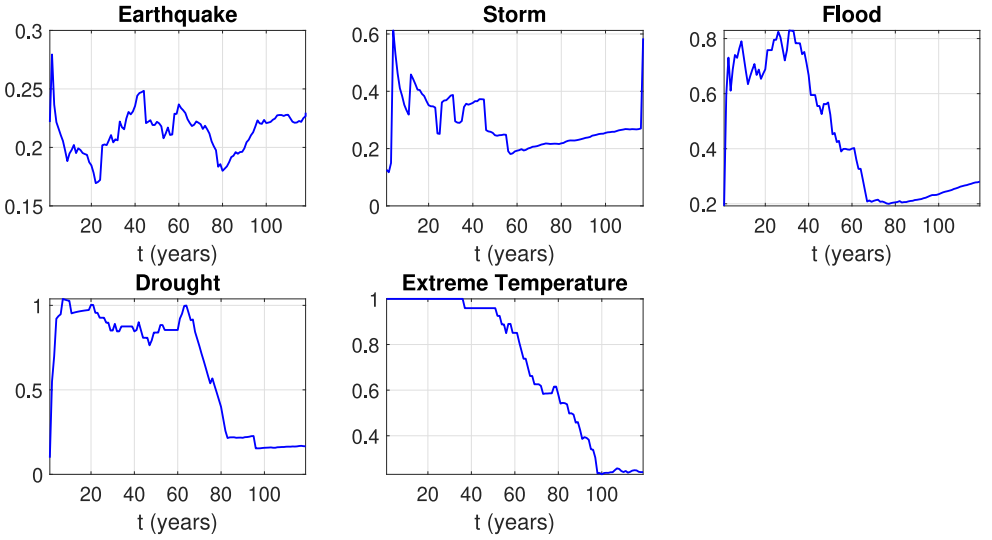

Fig. 3. The ratio between the variables f_t and x_t (as defined in Eq. (1)), with f_t computed similarly to x_t, replacing losses with occurrences. Notice that the most significant impact of climate change relates to floods, droughts, and extreme temperatures.

Table 3
Hurst exponent for log-losses of natural disasters.

Earthquake	Storm	Flood	Drought	Ext. Temp.
0.0887	0.2026	0.1287	0.1528	0.0964

The Hurst exponent "is robust with few assumptions about the underlying system, it has broad applicability for time series analysis" (Qian & Rasheed, 2004) moreover is a "robust statistic for testing the presence of noncyclic long-run statistical dependence" (Mandelbrot & Wallis, 1969). For those reasons, the H_e has been employed in various fields. For instance, Mandelbrot and Van Ness (1968) applied it when modeling, through fractional Brownian motions, strong interdependence between distant samples in natural time series.

In finance the Hurst exponent is around 0.5 (Nawrocki, 1995), (Qian & Rasheed, 2004), but it varies a lot depending on the market sentiments leading to "some episodes alternating low and high persistent behavior" (Alvarez-Ramirez, Alvarez, Rodriguez, & Fernandez-Anaya, 2008) occurring in correspondence of downturns.

Concerning natural disasters, the H_e is around 0.24, which "indicates that these time series are fractal and relatively long-term" anti-persistent (Jin et al., 2008). On our end, we confirm what has been reported in the literature (see Table 3).

A low level of the Hurst exponent indicates that the strength of mean-reverting does increase. For this reason, we selected a generalized two-factor square-root model that, in our opinion, matches the above-specified features. By doing that we take some inspiration from observing electricity spot prices. In that context, for example, an Ornstein–Uhlenbeck process, i.e. a mean-reverting drift damping model, has been used for modeling volatility persistence and anti-correlation (Rypdal & Løvsletten, 2013). By drawing this parallel, for forecasting losses due to natural disasters, we link up with the set of tools available for financial analysis and risk management.

3.2. A generalized two-factor square-root model

To introduce our generalized two-factor square-root model, let us start by denoting with $\{x_t\}_{t\geq 0}$ and $\{\sigma_t\}_{t\geq 0}$, respectively, the log-losses process due to natural disasters and the corresponding volatility. Assume that the dynamics of these processes, defined on a given a filtered probability space $(\Omega, \mathcal{F}, \{\mathcal{F}_t\}_{t\geq 0}, \mathbb{P})$, endowed with the filtration $\{\mathcal{F}_t\}_{t\geq 0}$ satisfying the usual hypothesis, evolves like a generalized two-factor square-root model defined as follows

$$\begin{cases} dx_t = k(\theta - x_t)dt + \alpha\sqrt{|x_t\sigma_t|}\, dW_t^x & x_0 > 0 \\ d\sigma_t = \delta(\gamma - \sigma_t)dt + \eta\sqrt{\sigma_t}\, dW_t^\sigma & \sigma_0 > 0, \end{cases} \tag{2}$$

where $k, \theta, \alpha, \delta, \gamma, \eta$ are strictly positive constants $\{W_t^x\}_{t\geq 0}$ and $\{W_t^\sigma\}_{t\geq 0}$ are two correlated Brownian motions, i.e.

$$dW_t^x dW_t^\sigma = \rho\, dt \qquad t \geq 0,$$

and $\rho \in (-1, 1)$. We can write

$$W_t^x = \rho W_t^\sigma + \sqrt{1-\rho^2}\, B_t, \tag{3}$$

where $\{B_t\}_{t\geq 0}$ is a standard Brownian motion independent of $\{W_t^{\sigma}\}_{t\geq 0}$. Thus system (2) reads as

$$\begin{cases} dx_t = k(\theta - x_t)dt + \alpha\sqrt{|x_t\sigma_t|}\,(\sqrt{1-\rho^2}\,dB_t + \rho dW_t^{\sigma}) & x_0 > 0 \\ d\sigma_t = \delta(\gamma - \sigma_t)dt + \eta\sqrt{\sigma_t}\,dW_t^{\sigma} & \sigma_0 > 0, \end{cases} \tag{4}$$

Assume from now on the Feller condition

$$2\delta\gamma \geq \eta^2. \tag{5}$$

Proposition 3.1. *Under condition (5) there exists a unique strong solution, $\{x_t, \sigma_t\}_{t\geq 0}$, to system (2) with state space $[0,+\infty)\times(0,+\infty)$. Moreover, there exists a random time $T > 0$ $\mathbb{P}$-a.s. such that the solution over the interval $[0,T]$ takes values in $(0,+\infty)^2$.*

Proof. *(i) existence and uniqueness of solution*

For any initial condition $\sigma_0 > 0$ the second equation in system (2) defines the dynamic of a CIR process, $\{\sigma_t\}_{t\geq 0}$, which is strictly positive (see, for instance Section 6.3.1 in Jeanblanc, Yor, and Chesney (2009)).

Define for any N natural number greater than σ_0

$$\tau_N = \inf\{t \geq 0 : \sigma_t > N\},$$

and observe that the sequence of stopping times $\{\tau_N\}_{N>\sigma_0}$ is increasing and τ_N goes to $+\infty$ as $N \to +\infty$ (because $\{\sigma_t\}_{t\geq 0}$ does not explode).

Let $\sigma_x(t,x,\omega) := \alpha\sqrt{\sigma_t(\omega)}\sqrt{|x|}$ the stochastic diffusion coefficient of the first equation in system (2). Observe that $\forall t \in [0,\tau_N(\omega)], \omega \in \Omega$

$$|\sigma_x(t,x,\omega) - \sigma_x(t,x',\omega)|^2 \leq \alpha^2 N|x - x'|.$$

We can now apply Theorem 1.5.5.1 (ii) in Jeanblanc et al. (2009), in fact, denoting $\varphi_N(x) = \alpha^2 N x$, the conditions required in Theorem 1.5.5.1 are satisfied, that is

$$\int_0^{+\infty} \frac{1}{\varphi_N(x)}dx = +\infty,$$

and $b(x) = k(\theta - x)$ is Lipschitz continuous in $x \in \mathbb{R}$. Thus for every N natural number such that $N > \sigma_0$, there exists a unique strong solution, $\{x_t^N\}_{0\leq t\leq \tau_N}$, to the first SDE in system (2) over the stochastic interval $[0,\tau_N]$.

Finally, notice that $x_t^{N+1} = x_t^N$, $t \in [0,\tau_N]$ and letting $N \to +\infty$ we obtain existence and uniqueness of the solution to the first SDE in system (2) $\{x_t\}_{t\geq 0}$, such that $x_t = x_t^N$, $t \in [0,\tau_N]$.

(ii) Positivity of solution

By a comparison result (see Theorem 1.5.5.9 in Jeanblanc et al. (2009)), since $k(\theta - x) \geq -kx$ and the solution to the following SDE

$$dX_t = -kX_t dt + \alpha\sqrt{|X_t\sigma_t|}\,dW_t^x, \quad X_0 = 0$$

is $X_t = 0$, $\forall t \geq 0$, we get that the process $\{x_t\}_{t\geq 0}$ takes values in $[0,+\infty)$.

Finally, since $x_0 > 0$ and $\{x_t\}_{t\geq 0}$ has continuous trajectories there exists a random time $T > 0$ such that

$$\mathbb{P}(x_t > 0, \quad \forall t \in [0,T]) = 1$$

and this concludes the proof. □

Two-factor models like the one in Eq. (2) have advantages and disadvantages that should be considered in terms of the intended use before selecting one of them. For example, to preserve the analytical tractability, the CIR2++ (the shifted additive two-factor CIR model, see Eqs. (4.1), (4.3), Chapter 4. in Brigo and Mercurio (2006)) has set $\rho = 0$. Without that, starting from the short-rate factors, it is not possible to compute analytically bond prices and rates. This is because the square-root non-central chi-square processes "do not work as well as linear-Gaussian processes when adding nonzero instantaneous correlations" (Brigo & Mercurio, 2006). The CIR2++ model has some advantages over the G2++ model, including its ability to maintain positive rates with reasonable parameter restrictions and its fatter tails. However, the G2++ model is more analytically tractable and easier to implement, making it more suitable for practical applications.

In our setting, a possible way to reduce the negative impact of the non-zero correlation ρ on the numerical tractability is given by the following results.

Lemma 3.2. *Let $\{x_t,\sigma_t\}_{t\in[0,T]}$ the unique strong solution to system (4) which takes values in $(0,+\infty)^2$. Consider the functions*

$$g(y) = \int_0^y \frac{1}{\sqrt{u}}\,du = 2\sqrt{y}, \qquad f(y) = \frac{\alpha}{\eta}\,y \qquad y \in \mathbb{R}_+.$$

Then, the process

$$p_t = g(x_t) - \rho f(\sigma_t) = 2\sqrt{x_t} - \frac{\alpha\rho}{\eta}\sigma_t \tag{6}$$

solves the following SDE, $\forall t \in [0,T]$

$$dp_t = h(x_t,\sigma_t)dt + \alpha\sqrt{\sigma_t(1-\rho^2)}\,dB_t \quad p_0 = 2\sqrt{x_0} - \frac{\alpha\rho}{\eta}\sigma_0, \tag{7}$$

where

$$h(x,\sigma) = \frac{k(\theta-x)}{\sqrt{x}} - \frac{\alpha^2\sigma_t}{4\sqrt{x}} - \frac{\rho\alpha\delta(\gamma-\sigma)}{\eta}. \tag{8}$$

Proof. By virtue of the Itô's formula (see, e.g., Shreve, 2004, Section 4.4.2) we get

$$dg(x_t) = \frac{1}{\sqrt{x_t}}dx_t - \frac{\alpha^2 x_t\sigma_t}{4x_t\sqrt{x_t}}\,dt = \left(\frac{k(\theta-x_t)}{\sqrt{x_t}} - \frac{\alpha^2\sigma_t}{4\sqrt{x_t}}\right)dt + \alpha\sqrt{\sigma_t}\,dW_t^x, \tag{9}$$

and

$$df(\sigma_t) = \frac{\alpha}{\eta}\,d\sigma_t = \frac{\alpha\delta(\gamma-\sigma_t)}{\eta}dt + \alpha\sqrt{\sigma_t}\,dW_t^\sigma. \tag{10}$$

If substitute (3) and (10) in (9), obtain

$$dg(x_t) = \left(\frac{k(\theta-x_t)}{\sqrt{x_t}} - \frac{\alpha^2\sigma_t}{4\sqrt{x_t}}\right)dt + \alpha\sqrt{\sigma_t}\,(\rho dW_t^\sigma + \sqrt{1-\rho^2}\,dB_t) =$$
$$\left(\frac{k(\theta-x_t)}{\sqrt{x_t}} - \frac{\alpha^2\sigma_t}{4\sqrt{x_t}} - \frac{\rho\alpha\delta(\gamma-\sigma_t)}{\eta}\right)dt + \rho df(\sigma_t) + \alpha\sqrt{\sigma_t(1-\rho^2)}\,dB_t,$$

i.e.,

$$dp_t = d\big(g(x_t) - \rho f(\sigma_t)\big) = h(x_t,\sigma_t)dt + \alpha\sqrt{\sigma_t(1-\rho^2)}\,dB_t. \quad \square$$

We are now in the position to restate system (4).

Theorem 3.3. *System (4) is equivalent to the following*

$$\begin{cases} dp_t = \widetilde{h}(p_t,\sigma_t)dt + \alpha\sqrt{\sigma_t(1-\rho^2)}\,dB_t \quad p_0 \in \mathbb{R} \\ d\sigma_t = \delta(\gamma-\sigma_t)dt + \eta\sqrt{\sigma_t}\,dW_t^\sigma, \quad \sigma_0 > 0 \end{cases} \tag{11}$$

where

$$\widetilde{h}(p,\sigma) = h\Big(\frac{1}{4}\big(p + \rho\frac{\alpha}{\eta}\sigma\big)^2, \sigma\Big) \tag{12}$$

and h *given in* (8).

(i) Let $\{x_t,\sigma_t\}_{t\in[0,T]}$ *be a strong solution to* (4) *with initial condition* $(x_0,\sigma_0) \in (0,+\infty)^2$ *and with state-space* $(0,+\infty)^2$. *Then there exists* $0 < T' \le T$ *such that* $\{p_t,\sigma_t\}_{t\in[0,T']}$, *with* p_t *defined in* (6), *solves system* (11) *with initial condition* $(p_0 = 2\sqrt{x_0} - \frac{\alpha\rho}{\eta}\sigma_0, \sigma_0)$.

(ii) Let $\{p_t,\sigma_t\}_{t\in[0,T]}$ *be a strong solution to* (11) *with initial condition* $(p_0,\sigma_0) \in (0,+\infty)^2$ *and such that* $p_t + \rho\frac{\alpha}{\eta}\sigma_t > 0$, $\forall t \in [0,T]$. *Then* $\{x_t,\sigma_t\}_{t\in[0,T]}$, *with* $x_t = \frac{1}{4}\big(p_t + \rho\frac{\alpha}{\eta}\sigma_t\big)^2$, *solves system* (4) *with initial condition* $(x_0 = \frac{1}{4}\big(p_0 + \rho\frac{\alpha}{\eta}\sigma_0\big)^2, \sigma_0)$. *Moreover* $\{x_t,\sigma_t\}_{t\in[0,T]}$ *has state-space in* $(0,+\infty)^2$.

Proof. (*i*). By Proposition 3.1 the process $\{p_t\}_{t\in[0,T]}$, defined in (6), solves the SDE in (7) over the stochastic interval $[0,T]$. Since $p_0 + \frac{\alpha\rho}{\eta}\sigma_0 = 2\sqrt{x_0} > 0$ and the processes, $\{p_t\}_{t\in[0,T]}$ and $\{\sigma_t\}_{t\in[0,T]}$ have continuous sample paths there exists ar random time T', such that $0 < T' \le T$ and $p_t + \frac{\alpha\rho}{\eta}\sigma_t > 0$, $\forall t \in [0,T']$. Hence by (6) we get that $2\sqrt{x_t} = p_t + \frac{\alpha\rho}{\eta}\sigma_t$ and $x_t = \frac{1}{4}\big(p_t + \rho\frac{\alpha}{\eta}\sigma_t\big)^2$ which inserted in Eq. (8) leads to Eq. (12).

(*ii*). Let $\{p_t,\sigma_t\}_{t\in[0,T]}$ be a strong solution to (11) with initial condition $(p_0,\sigma_0) \in (0,+\infty)^2$ and such that $p_t + \rho\frac{\alpha}{\eta}\sigma_t > 0$, $\forall t \in [0,T]$. Let us define $x_t = \frac{1}{4}\big(p_t + \rho\frac{\alpha}{\eta}\sigma_t\big)^2$, $\forall t \in [0,T]$. From Itô's formula we get that the pair $\{x_t,\sigma_t\}_{t\in[0,T]}$ solves system (4) with initial condition $(x_0 = \frac{1}{4}\big(p_0 + \rho\frac{\alpha}{\eta}\sigma_0\big)^2, \sigma_0)$. By construction $x_t > 0$ $\forall t \in [0,T]$, hence the state space of $\{x_t,\sigma_t\}_{t\in[0,T]}$ is $(0,+\infty)^2$. $\square$

Remark 3.4. Notice that as consequence of Proposition 3.1 by strong existence and uniqueness of solution to system (4), over a stochastic interval $[0,T]$ and with state-space $(0,+\infty)^2$, we get strong existence and uniqueness of solution to system (11) over a stochastic interval $[0,T']$ $(T' \le T)$, such that $p_t + \rho\frac{\alpha}{\eta}\sigma_t > 0$, $\forall t \in [0,T']$.

The above function g in (6) represents the so-called *Lamperti's transformation*. Theorem 3.3 introduces a new auxiliary process, $\{p_t\}_{t\in[0,T]}$, which is not correlated with $\{\sigma_t\}_{t\ge0}$. This fact allows a fast and independent simulation of the process $\{x_t\}_{t\ge0}$; indeed, one can simulate $\{\sigma_t\}_{t\ge0}$ and $\{p_t\}_{t\ge0}$ separately and finally may compute $\{x_t\}_{t\ge0}$ as

$$x_t = g^{-1}(p_t + \rho f(\sigma_t)) = \frac{1}{4}\left(p_t + \frac{\alpha\rho}{\eta}\sigma_t\right)^2. \tag{13}$$

3.3. Baseline models

In this Section four baseline models for comparison and benchmarking are considered as alternative candidates to system (2) for modeling log-losses of natural disasters. Namely, the first-order autoregressive AR(1) model, the two-factor Gaussian model G2++, the extreme value distribution model (EVM) and the generalized linear regression model (GLM). The AR(1) is pretty good at predicting the average loss and volatility of the stochastic process when more sophisticated models fail. The other three models are often used in insurance and finance for modeling and forecasting stochastic processes as mentioned in Section 2.

3.3.1. The first-order autoregressive AR(1) model

The AR(1) model is a representation of a short-memory random process satisfying the following equation:

$$Y_{t+1} = c + \Phi Y_t + \varepsilon_{t+1},$$

with c a given constant. The output random variable Y_{t+1} is assumed to depend linearly only on its previous value Y_t and on the current value of a white noise process ε_t with zero mean and constant variance $\sigma_\varepsilon^2 > 0$. The process is stationary if the parameter $\Phi \in (0, 1)$.

The AR(1) model has been already used in modeling and understanding the persistence of climate variability (Vyushin, Kushner, & Zwiers, 2012). Moreover, it can be considered as the discrete-time analogue of the mean-reverting Ornstein–Uhlenbeck (OU) process

$$dY_t = \chi(\mu - Y_t)dt + \lambda dW_t,$$

where $\chi > 0$, μ and λ are constants. Indeed, when the Ornstein–Uhlenbeck process is sampled at equally spaced time intervals $[t, t + \Delta]$, we get

$$Y_{t+\Delta} = c + \Phi Y_t + \varepsilon_{t+\Delta},$$

with

$$\Phi = e^{-\chi\Delta}, \quad c = (1 - \Phi)\mu, \quad \varepsilon_{t+\Delta} \sim N\left(0, \frac{\lambda^2}{2\chi}(1 - \Phi^2)\right).$$

The conditional distribution of the OU process is normal with parameters

$$\mathbb{E}[Y_{t+n\Delta}|Y_t] = \mu(1 - \Phi^n) + Y_t\,\Phi^n$$

and

$$\text{Var}\,(Y_{t+n\Delta}|Y_t) = \frac{\lambda^2}{2\chi}(1 - \Phi^{2n}).$$

3.3.2. The G2++ model

The G2++ model is a two-factor Gaussian model where the state process is the sum of two correlated Gaussian factors plus a deterministic function chosen to fit the observed real data exactly. Due to its analytic tractability, explicit formulas for its distribution and moments can be easily derived. Gaussian models, such as the G2++, are widely used in practice due to their practical usefulness. For more details see Brigo and Mercurio (2006, Chapter IV).

Under this model, the principal process Y_t is expressed as the sum

$$Y_t = r_t + q_t + \varphi(t),$$

where the processes $\{r_t\}_{t\geq 0}$ and $\{q_t\}_{t\geq 0}$ satisfy

$$\begin{cases} dr_t = -a\,r_t dt + \psi\,dW_t^r & r_0 > 0 \\ dq_t = -b\,q_t\,dt + \zeta\,dW_t^q, & q_0 > 0 \end{cases} \tag{14}$$

with $\{W_t^r\}_{t\geq 0}$, $\{W_t^q\}_{t\geq 0}$ correlated Brownian motion such that $dW_t^r dW_t^q = \rho\,dt$, $\rho \in (-1, 1)$ and a, ψ, b, ζ are positive constants. In particular, the model fits the observed data if and only if (Brigo & Mercurio, 2006, Corollary 4.2.1)

$$\begin{aligned}\varphi(t) \;=\; & f_s(t) + \left(\frac{\psi}{2a}\left(1 - e^{-at-s}\right)\right)^2 + \left(\frac{\zeta}{2b}\left(1 - e^{-b(t-s)}\right)\right)^2 \\ & + \rho\frac{\psi\zeta}{a\,b}\left(1 - e^{-a(t-s)}\right)\left(1 - e^{b(t-s)}\right),\end{aligned}$$

where $f_s(t)$ denotes the instantaneous forward value of Y_t evaluated from s and t. Notice that we ignore such term $f_s(t)$, according to Brigo and Mercurio (2006, Remark 4.2.1).

Denoted by $\{\mathcal{F}_t\}_{t\geq 0}$ the filtration generated by the Brownian motions $\{W_t^r\}_{t\geq 0}$, $\{W_t^q\}_{t\geq 0}$, it can be shown that for any $0 \leq s < t$, X_t conditional on $\mathcal{F}_s$ is normally distributed with mean

$$\mathbb{E}[Y_t|\mathcal{F}_s] = r_s e^{-a(t-s)} + q_s e^{-b(t-s)} + \varphi(t), \tag{15}$$

and variance

$$\text{Var}\,(Y_t|\mathcal{F}_s) = \frac{\psi^2}{2a}\left(1-e^{-2a(t-s)}\right)+\frac{\zeta^2}{2b}\left(1-e^{-2b(t-s)}\right) +2\rho\left(\frac{\psi\,\zeta}{a+b}\right)\left(1-e^{-(a+b)(t-s)}\right). \tag{16}$$

3.3.3. The extreme value distribution model (EVM)

Extreme value distributions are widely used in finance because they can effectively model extreme events that cannot be represented by other distributions such as the Gaussian, which has tails that decay exponentially quickly.

Given the location parameter a_1 and scale parameter a_2, the probability density function for the extreme value distribution is given by

$$y = f(x|a_1,a_2) = \frac{1}{a_2}e^{(x-a_1)/a_2-e^{(x-a_1)/a_2}}.$$

It can be observed that if X has a Weibull distribution with parameters $b_1 > 0$ and $b_2 > 0$, then $\log X$ has an extreme value distribution with parameters $a_1 = \log b_1$ and $a_2 = 1/b_2$.

3.3.4. Generalized linear model (GLM)

The last baseline model that we introduce for comparison is the generalized linear model (GLM) that we use for nonlinear prediction (NLP)

$$y = c_1 + c_2 e^{-c_3 x} \tag{17}$$

where c_1, c_2 and c_3 are some parameters we calibrate by means of a nonlinear least squares regression. Eq. (17) is consistent with the G2++, is an industry standard (see De Jong & Heller, 2008; Goldburd, Khare, & Tevet, 2016; Ohlsson & Johansson, 2010) and, in our tests, performed well in fitting data. We have run a robust estimation with the iteratively reweighted least squares algorithm (Holland & Welsch, 1977) which, at each iteration, recalculates the weights based on the residual from the previous iteration. This process progressively downweights outliers and iterations continue until the weights converge.

3.4. Numerical implementation

3.4.1. Forecasting the expected value

As explained in Section 2, many candidate models have been tested, but we found that a two-factor model to describe the dynamics of financial log-losses and their volatility is the best compromise between tractability and efficiency. In particular, the novelty of the proposed model (2) consists in a nonzero correlation ρ between the two processes x_t and σ_t. Indeed, in contrast with a two-factor Gaussian model, which is more analytically tractable, the two-factor square-root model becomes analytically unmanageable if $\rho \neq 0$ (see, for instance, the G2, G2++, CIR2 and CIR2++ models described in Brigo and Mercurio (2006)).

Having said that, if $\rho \neq 0$, no closed formula is known for the transition density of x_t. As a consequence, the conditional expected values of x_t and σ_t cannot be computed explicitly. This implies the necessity of resorting to numerical methods to generate forecasts within the framework of model (2).

Denote by $X_s = \{X_{s+1}, \dots \dots X_{s+N}\}$, $s > 0$, a time series of N observed realizations of the process $\{x_t\}_{t\geq 0}$. Moreover, consider a window, $\mathcal{I}_t$, of fixed size L, that is rolled through time $t \geq 0$. The length of this window is the historical period over which we calibrate our parameter vectors $\nu_t^x := (k_t, \theta_t, \alpha_t)$ and $\nu_t^\sigma := (\delta_t, \gamma_t, \eta_t)$, for any time t.

In order to simulate the volatility process σ_t, we construct a time series, V_s, of "pointwise" volatilities, obtained as the pointwise difference in absolute value between X_s and the corresponding exponential moving average (EWMA) E_s, that is

$$V_{s+u} = |X_{s+u} - E_{s+u}|, \quad 1 \leq u \leq N. \tag{18}$$

The aforementioned time series provides a more precise measure of variability in the process x_t compared to other statistics, such as the sample standard deviation, since it takes into account the temporal aspect of the data.

We use the time series V_s to calibrate the parameter vector ν_t^σ on the rolling window $\mathcal{I}_t$ by applying the maximum likelihood (ML) estimation method, implemented in Matlab, to estimate the parameters of the CIR process (see Kladıvko, 2007). In financial literature, there exist different and more sophisticated methodologies to estimate the parameter of ergodic diffusion processes (see, e.g., Orlando et al., 2019c, Section 4.4) but they require rolling windows of size greater than L to be efficient.

Following the algorithm proposed in Kladıvko (2007), the ML estimate $\widehat{\nu}_t^\sigma = (\widehat{\delta}_t, \widehat{\gamma}_t, \widehat{\eta}_t)$ is obtained by solving the following optimization problem

$$\widehat{\nu}_t^\sigma = \arg\left(\max_{\nu_t^\sigma} \ln \mathcal{L}(\nu_t^\sigma)\right). \tag{19}$$

Notice that $\ln \mathcal{L}(\nu_t^\sigma)$ denotes the log-likelihood function of the CIR process

$$\ln \mathcal{L}(\nu_t^\sigma) = \sum_{u=1}^{L-1} \mathcal{P}(V_{s+h+u+1}|V_{s+h+u}) \qquad (h \geq 1),$$

computed on the window $\mathcal{I}_t = \{V_{s+h+1}, \dots, V_{s+h+L}\}$, $t = s + h + L$, and $\mathcal{P}$ is the transition density of the CIR process (see Jeanblanc et al., 2009, Proposition 6.3.2.1). To ensure the convergence to the ML estimates, the ordinary least-squares (OLS) regression method is used to determine the initial parameter estimates.

The predicted future volatility value σ^F_{t+u}, $u \geq 1$, may be computed by the CIR conditional expectation

$$\sigma^F_{t+u} = \mathbb{E}[\sigma_{t+u}|\sigma_t] = \widehat{\gamma}_t + (V_t - \widehat{\gamma}_t)e^{-\widehat{\delta}_t u} \qquad (u \geq 1), \tag{20}$$

where V_t is the observed volatility corresponding to σ_t.

The estimate of the parameter vector $\widehat{\nu}^x_t$ on the rolling window $\mathcal{I}_t$ is obtained using the same procedure above described by using the time series X_s. The sample autocorrelation of X_s on $\mathcal{I}_t$, $\widehat{\rho}_t$, with lag equal to -1, is considered as an estimate of the correlation coefficient ρ_t. It is important to note that, in this context, the correlation is time-dependent, as it changes with each new calibration.

In order to forecast the future value x^F_{t+u}, $u \geq 1$, we applied the second-order Milstein discretization scheme according to (Orlando et al., 2019c, Section 4.5) to simulate the auxiliary process p_t (see (6)) and σ_t observed at m equidistant points in the interval $[t, t+u]$:

$$\begin{cases} \sigma^S_{t_{i+1}} = \sigma^S_{t_i} + \widehat{\delta}_t(\widehat{\gamma}_t - \sigma^S_{t_i})\Delta + \widehat{\eta}_t\sqrt{\sigma^S_{t_i}\Delta}\, W^\sigma_{t_i} + \frac{\widehat{\eta}^2_t}{4}\left[\left(\sqrt{\Delta}\, W^\sigma_{t_i}\right)^2 - \Delta\right], \\ p^S_{t_{i+1}} = p^S_{t_i} + h\left(g^{-1}(p^S_{t_i} + \widehat{\rho}_t f(\sigma^S_{t_i})), \sigma^S_{t_i}\right)\Delta + \widehat{\omega}_t\sqrt{\sigma^S_{t_i}(1-\widehat{\rho}^2_t)\Delta}\, B_{t_i} + \frac{(\widehat{\omega}_t\sigma^S_{t_i}(1-\widehat{\rho}^2_t))^2}{4}\left[\left(\sqrt{\Delta}\, B_{t_i}\right)^2 - \Delta\right], \end{cases} \tag{21}$$

where f, g, h are defined by (6), (8), respectively, and $\Delta = t_{i+1} - t_i$ is the time-step, being $t = t_1 < t_2 < \cdots \dots < t_m = t + u$. The initial values of the simulated sample paths have been set $(p^S_t, \sigma^S_t) = (P_t, V_t)$, where (P_t, V_t) denote the corresponding observations in the time series P_s[1] and V_s, respectively.

Following this procedure, we simulated $h = 100,000$ trajectories (p^S, σ^S). Then, the predicted future value p^F_{t+u}, is obtained averaging over the 100,000 corresponding simulated values, that is

$$p^F_{t+u} = \frac{1}{h}\sum_{i=1}^{h} p^S_{t+u,i}. \tag{22}$$

Finally, from relation (13), we get

$$x^F_{t+u} = g^{-1}\left(p^F_{t+u} + \widehat{\rho}_t f(\sigma^F_{t+u})\right). \tag{23}$$

3.4.2. Forecasting the extreme value (VaR)

As tested in Section 4, the forecasted future values provide a good approximation of the expected values of the financial log-losses and the corresponding volatility. To avoid future observation exceeding a given high level, an upper bound of predictions x^F_{t+u} is needed to ensure the 99% confidence level Value at Risk (VaR).

For this reason, we define a correction term as the following random variable

$$z_{t+u} := x_{t+u} - (x^F_{t+u} + \sigma^F_{t+u}), \quad u \geq 1. \tag{24}$$

In other terms, as the distribution of losses is not normal, the correction term z_{t+u} is what we require to get our VaR with a confidence level of 99%. The realization of the random value z_{t+u} is denoted with Z_{t+u} so that the upper bound VaR_{GPD} of the prediction x^F_{t+u} is

$$VaR_{GPD} = x^F_{t+u} + \sigma^F_{t+u} + Z_{t+u}. \tag{25}$$

As we intend to model the extreme values, we assume that Z_{t+u} follows a Generalized Pareto Distribution (GPD), a probability distribution introduced by Pickands III (1975) as a model for tails. The cumulative distribution function is given by, for all $y > 0$

$$G(y) = \begin{cases} 1 - \left(1 + \frac{\xi y}{\beta}\right)^{-\gamma}, & \text{if } \xi > 0, \\ 1 - e^{-\frac{y}{\beta}}, & \text{if } \xi = 0, \end{cases} \tag{26}$$

where ξ, and $\beta > 0$ are the so-called shape and scale parameters, respectively, and $\gamma = 1/\xi$ is the tail index parameter.

To estimate the unknown GPD parameters (ξ, β) we adopted the following procedure. Given the initial rolling window $\mathcal{I}_t = \{X_{s+1}, \dots \dots X_{s+L}\}$, where $t = s + L$, used to estimate the parameter vectors ν^σ_t, ν^x_t as above-described, consider a second fixed window $\mathcal{I}'_t = \{X_{s+L+1}, \dots \dots X_{s+L'}\}$ with initial size $L' > L$ on which we compute the estimates $(\widehat{\xi}_t, \widehat{\beta}_t)$. Then a realization, Z_{t+u}, of the correction term z_{t+u} is estimated by the sample mean computed over 100,000 simulated random variables with GPD and parameters $(\widehat{\xi}_t, \widehat{\beta}_t)$. Note that in the next steps, while the window $\mathcal{I}_t$ rolls through time, each year adding a new observation and taking off the oldest one, a new observation is added each time to the window $\mathcal{I}'_t$. As a consequence, the size L' of $\mathcal{I}'_t$ increases each time by one year. This is to avoid too large variations in the computation of the correction term that may cause a shortfall of capital for insurers.

[1] $P_s = g(X_s) - \rho_s f(V_s)$.

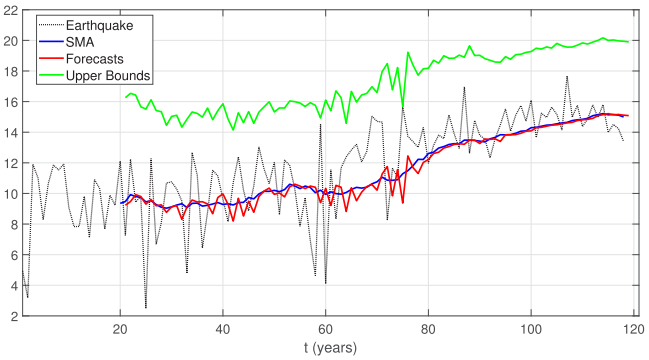

Fig. 4. Earthquake Forecasts. The (dotted) black line is the log-losses of the natural disaster X_t, the blue line is its SMA (ex post), the red line represents the corresponding forecasts x_t^F; finally, the green line refers to the upper bound VaR_{GPD} computed as $x_t^F + \sigma_t^F + Z_t$ with $L' = 119$. Out-of-sample forecasts. (For interpretation of the references to color in this figure legend, the reader is referred to the web version of this article.)

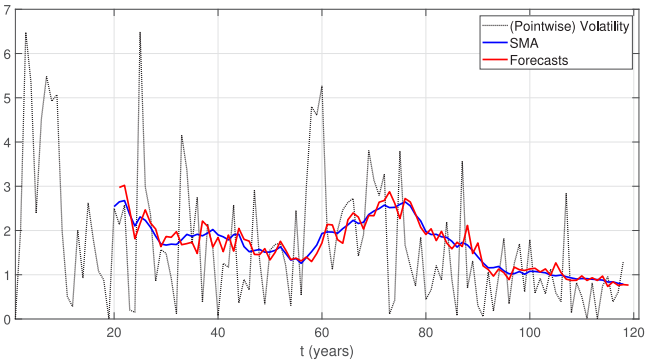

Fig. 5. Earthquake volatility Forecasts. The black (dotted) line is the (pointwise) volatility of the log-losses of disaster V_t, the blue line is its SMA (ex post), the red line represents the corresponding forecasts σ_t^F. (For interpretation of the references to color in this figure legend, the reader is referred to the web version of this article.)

3.4.3. Example on earthquake forecasts

In the figure shown in Fig. 4, the log losses of a natural disaster are represented by a dotted black line. This line exhibits erratic and unpredictable behavior, which poses a challenge for insurers who aim to estimate the expected losses over time. To address this challenge, a simple moving average (SMA) is calculated based on the realized occurrences of losses and is represented by the blue line. Note that in our method, the SMA includes 20 points, as determined by the rolling window size set to $L' = 20$. Initially calibrated with L = 10 (equivalent to ten years), we progressively increase L by one each subsequent year (i.e., with each data point) until it reaches 20. In addition, the forecasts calculated with Eq. (2) (red line) and upper bound (green line) are shown. The upper bound represents the value at risk (VaR) for the model used (described in Section 3.4.2) and is obtained using the generalized Pareto distribution (GPD) and the methodology outlined in Section 3.4. The graph illustrates that the model is very close to the SMA and, except for one exception over 119 years, consistently predicts losses that are higher than the peaks of realized losses.

In addition to evaluating the logarithmic losses, we intend to estimate their average volatility. This is of particular importance from a firm standpoint as the aim is not only to ensure solvency but, also, to deliver a regular stream of cash flow to the shareholders by avoiding excessive variations due to reserves' volatility. Fig. 5 presents a comparison between the average ex-post volatility of logarithmic losses, represented by the simple moving average (SMA) in blue, and our ex-ante forecast in red. As can be observed, our forecast is in good agreement with the realized volatility, which provides support to the accuracy of our model.

In this context, Z_t is a correction term that is added to both the occurrences and the volatility. The value of this term varies based on the window size, and it can significantly impact the values presented in Tables 5, 6, 9 in Section 4. Fig. 6 illustrates how the correction term can change drastically when the window size exceeds 50. To strike a balance between size and stability, we chose a window size of 20.

Finally, while standard techniques based on extreme value theories produce 5-year forecasts, in Fig. 7 we demonstrate the versatility of our model which can preserve its predicting power over longer horizons (e.g. 10 and 15 years).

3.5. Accuracy statistics for model predictions

As a measure of accuracy, we adopt the following statistics:

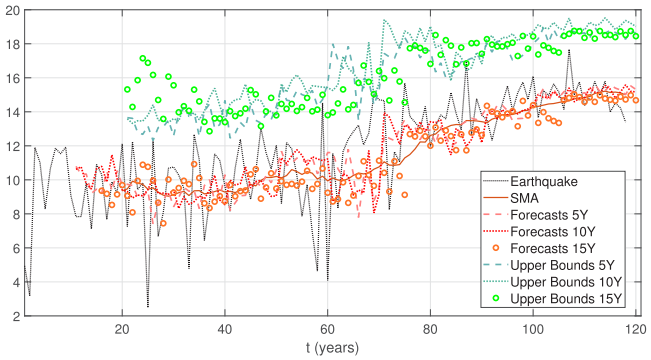

Fig. 6. Percentage variation of Z_t for different initial window size $L' \geq 20$, for any $t \geq L'$.

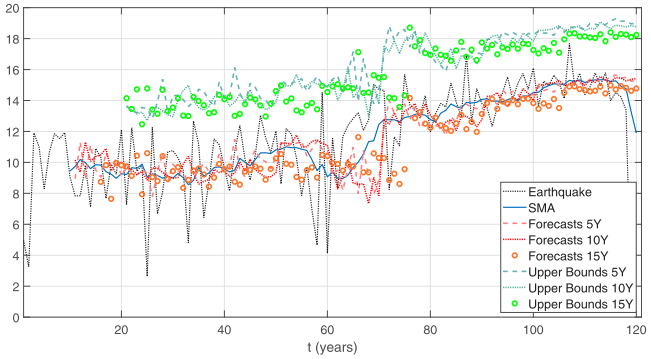

Fig. 7. Earthquake log-losses forecasts for the next 5, 10 and 15 years.

Table 4
MAPE accuracy levels.

MAPE	Forecasting level
$< 10\%$	High
$10\% - 20\%$	Good
$20\% - 50\%$	Resonable
$> 50\%$	Inaccurate

- The root mean squared error (RMSE), defined as

$$RMSE = \sqrt{\frac{1}{N}\sum_{h=1}^{N} e_h^2}, \tag{27}$$

with e_h representing the residuals between the observed data and their corresponding predictions, computed over N observations. The residual term reflects how close the predicted values are to the actual observed data, where values close to zero indicate a good match, and values close to one indicate poor performance. To mitigate the impact of outliers, the normalized root mean squared error (NRMSE) is used instead. This is defined as follows

$$NRMSE = \frac{RMSE}{X_{max} - X_{min}}, \tag{28}$$

where X_{max} and X_{min} are the maximum and minimum values of the historical time series, respectively.
- The mean absolute percentage error (MAPE), defined below

$$MAPE = \frac{1}{N}\sum_{h=1}^{N}\left|\frac{e_h}{X_h}\right|. \tag{29}$$

Table 4 suggests the accuracy levels of the MAPE criterion.

3.6. Backtesting on exceedances for model validation

To check if a model can meet the expected maximum allowed exceptions, we recur the range of tools available to risk management. We said that the upper bound of the GPD represents the maximum loss. Therefore, similarly to what financial institutions do to backtest their VaR, in the following we describe the most popular methods that we are going to use to validate our model.

3.6.1. Traffic light test (TLT)

The Traffic Light Test was proposed by the Basel Committee on Banking Supervision 1996, Balthazar (2006) for giving a green light on the adopted model and it is a variant of the binomial test. The TLT test, given a number of exceptions E, calculates the probability of observing from 0 to E exceptions.

3.6.2. Kupiec's POF test

This test borrows its name from Kupiec (1995) and it is a variant on the binomial test. The Kupiec test is also named the proportion of failures (POF) test because of how it is constructed. As well as the TLT test, the POF test is based on the binomial distribution but, additionally, it uses a likelihood ratio. This is to check if the probability of exceptions is synchronized with the probability p defined by the VaR confidence level. In case the frequency of exceptions over the backtested time series is different than p, the VaR is rejected.

3.6.3. Kupiec's TUFF tests

Kupiec proposed a second test called time until first failure (TUFF) (Jorion et al., 2009). The TUFF test examines the timing of the first failure occurrence. If the first failure occurs too early from a probabilistic standpoint, the VaR is considered rejected by the test. Since examining only the first failure can leave out important information regarding subsequent failures, the TUFF test was designed to consider all recorded failures.

3.6.4. Christoffersen's (CC) Interval Forecast Tests

The Interval Forecast Tests, also known as the CC tests, were introduced by Christoffersen (1998). The main concept behind these tests is to evaluate whether the probability of an exception occurring at a specific time is dependent on whether an exception has occurred previously. Unlike the unconditional probability of observing an exception, the CC tests focus solely on the relationship between consecutive time intervals.

4. Numerical results

4.1. Results on 1-year horizon

In this section we apply the procedure described in Section 3.4 to the Dataset described in Section 3.1. Detailed figures are reported in Appendix. We set the parameters L, L' and Δ equal to

$$L = 10Y, \quad L' = 20Y, \quad \Delta = \frac{1}{360}.$$

As a first step, we computed the NRMSE and MAPE statistics as a difference between the forecasted financial log losses due to natural disasters and the corresponding simple moving averages (SMA) (Table 5), and between the forecasted volatility and the corresponding simple moving averages (SMA) (Table 6). Further, we compare our results with the predictions given by the baseline models. As mentioned the AR(1) and the SMA are indicated to forecast smooth time series. Notice that the calibration of the G2++ model follows the techniques described in Section 3.4, where the processes r_t and q_t refer to X_t and V_t, respectively. This is because we focus on the variations instead of on the levels to keep them under control and, so, to avoid unexpected large losses for insurers. Notice that the expected log-losses and their volatility are predicted by formula (15) and (16), respectively.

To verify if the correction term Z_t provides a VaR at a 99% confidence level, we examine the percentage variation of the exceedances for all $t \geq L'$. By analyzing the percentage variation and exceedances for different sizes L' of the window $\mathcal{I}'_t$, with $L' \geq 20$, we can determine if smooth hedging is achieved without drastic jumps for insurance companies. Specifically, Table 8 presents the maximum percentage variation of Z_t and the minimum window size L' required to achieve the 99% VaR for all $t \geq L'$.

Additionally, the Kupiec (POF), Christoffersen (CC), and TUFF tests do not reject their null hypotheses at a 99% significance level, with the corresponding p-values and L-ratios presented in Table 7. It is noteworthy that the p-values and L-ratios are the same for each time series since they have the same number of observations, exceedances, and relative frequency. Moreover, the traffic light test results in a "green" category with a cumulative probability of failures amounting to 1.6%.

Table 5
NRMSE and MAPE between 1 year forecasts of log-losses and their SMA. The gray highlights the results obtained with model in Eq. (2). Out-of-sample results.

Forecasting error of considered models - Returns						
Horizon	Model Error	Earthquake	Storm	Flood	Drought	Ext. Temp.
1 Y	$NRMSE^{Eq.\ (2)}$	3.32%	4.80%	4.92%	4.54%	2.44%
	$NRMSE_{AR}$	24.14%	20.18%	14.30%	17.55%	9.10%
	$NRMSE_{G2}$	19.30%	12.46%	15.98%	19.05%	11.21%
	$NRMSE_{EVM}$	5.79%	4.48%	4.9%	19.05%	10.21%
	$NRMSE_{GLM}$	17.12%	5.94%	5.36%	7.18%	2.99%
1 Y	$MAPE^{Eq.\ (2)}$	4.77%	3.02%	5.87%	6.67%	3.02%
	$MAPE_{AR}$	6.59%	7.14%	18.24%	20.77%	12.16%
	$MAPE_{G2}$	7.66%	8.42%	22.78%	21.58%	14.34%
	$MAPE_{EVM}$	5.23%	3.13%	9.01%	10.23%	6.57%
	$MAPE_{GLM}$	8.01%	4.20%	13.35%	6.70%	2.91%

Table 6
NRMSE and MAPE between 1 year forecasts of the volatility of log-losses and their SMA. The gray highlights the results obtained with model in Eq. (2). Out-of-sample results.

Forecasting error of considered models - Volatility						
Horizon	Model Error	Earthquake	Storm	Flood	Drought	Ext. Temp.
1 Y	$NRMSE^{Eq.\ (2)}$	8.76%	9.24%	6.55%	9.85%	5.19%
	$NRMSE_{AR}$	53.10%	37.35%	18.77%	39.43%	44.56%
	$NRMSE_{G2}$	24.73%	13.75%	25.48%	45.63%	20.61%
	$NRMSE_{EVM}$	11.74%	8.49%	6.01%	9.6%	28.80%
	$NRMSE_{GLM}$	30.12%	24.52%	23.07%	33.45%	23.16%
1 Y	$MAPE^{Eq.\ (2)}$	5.10%	3.62%	3.60%	7.25%	2.88%
	$MAPE_{AR}$	11.48%	12.07%	11.13%	20.98%	26.88%
	$MAPE_{G2}$	12.13%	11.74%	20.68%	28.94%	10.50%
	$MAPE_{EVM}$	12.04%	11.71%	8.91%	14.23%	16.72%
	$MAPE_{GLM}$	35.27%	33.20%	31.31%	48.27%	38.19%

Table 7
99% VaR test response. Out-of-sample results.

	POF	CC	TUFF, TBFI
Response	"accept"	"accept"	"accept"
p-value	0.1542	0.3623	0.4297
L-ratio	2.0301	2.0301	4.0964

Table 8
Maximum percentage variation of Z_t and minimum L' giving the 99% confidence level VaR. Out-of-sample results.

	Earthquake	Storm	Flood	Drought	Ext. Temp.
Max. Variation	3.70%	3.25%	4.15%	3.26%	3.55%
Min. L'	61	20	20	23	55

4.2. Results on 5, 10 and 15-year horizon

In addition to 1-year forecasts, to highlight the power of our predictions, we apply the analysis to the next $5Y$, $10Y$ and $15Y$ horizons. As previously done, all forecasts are out-of-sample. We start with a window of ten data (from $T = 10Y$) and the results are listed in Table 9.

For the reason of space, graphs are in Appendix, where we show the forecasted series (relative to the next year or 5, 10 and 15 years) $x^F_{t+u}, \sigma^F_{t+u}$ and the percentage variation of Z_t for any natural disaster considered.

Notice that, as well as illustrated in Tables 5 and 6, we obtained similar results with regard to the volatility and the NRMSE. For the sake of readability, we do not show those results.

Finally, Table 10 shows the ML estimates with their confidence intervals.

5. Relevance for premia calculations

As mentioned, natural phenomena such as earthquakes, hurricanes and floods can have serious consequences for insurance companies, see eg. some empirical studies such as Born and Viscusi (2006), Benali and Feki (2017). Insurance companies offer their

Table 9
Different MAPE for 5, 10 and 15 years predictions. The gray highlights the results obtained with model in Eq. (2). Out-of-sample results.

Forecasting error of considered models - Returns						
Horizon	Model Error	Earthquake	Storm	Flood	Drought	Ext. Temp.
5 Y	$\text{MAPE}^{\text{Eq. (2)}}$	5.10%	6.23%	12.68%	20.60%	20.01%
	MAPE_{AR}	15.46%	14.68%	29.75%	34.34%	22.52%
	MAPE_{G2}	7.79%	8.45%	23.01%	26.70%	20.91%
	MAPE_{EVM}	5.91%	8.03%	22.73%	22.12%	20.84%
	MAPE_{GLM}	6.90%	7.88%	30.84%	24.37%	12.25%
10 Y	$\text{MAPE}^{\text{Eq. (2)}}$	5.32%	7.95%	17.60%	29.45%	21.45%
	MAPE_{AR}	16.46%	18.19%	28.75%	38.50%	54.05%
	MAPE_{G2}	7.90%	10.15%	26.59%	29.70%	25.25%
	MAPE_{EVM}	9.16%	12.85%	29.77%	36.91%	23.25%
	MAPE_{GLM}	11.23%	14.49%	46.64%	34.14%	23.95%
15 Y	$\text{MAPE}^{\text{Eq. (2)}}$	6.72%	10.25%	19.69%	32.68%	25.15%
	MAPE_{AR}	18.46%	22.19%	29.84%	42.04%	56.27%
	MAPE_{G2}	9.30%	10.92%	27.09%	39.70%	29.34%
	MAPE_{EVM}	11.14%	16.63%	31.99%	38.31%	26.11%
	MAPE_{GLM}	14.47%	28.97%	48.29%	35.42%	39.14%

Table 10
Earthquake simulations. Parameters estimations and their confidence intervals.

Parameter	Estimation	Confidence interval
δ	11.1052	[8.4354, 13.7750]
γ	1.9818	[1.6601, 2.3036]
η	6.4060	[5.6240, 7.1880]
k	1.0422	[0.9830, 1.1014]
θ	11.0976	[10.5315, 11.6637]
α	4.2469	[3.7285, 4.7653]

customers risk insurance in exchange for a premium. Therefore, the main challenge for actuaries is to find an optimal compromise between a reasonable premium aimed at guaranteeing profit margins and solvency to the insurance company and the need to offer competitive rates on the market. To this end, the assessment of premiums related to claims caused by natural disasters has become increasingly difficult due to global warming which increases both the probability and the severity of these phenomena.

The most popular premium calculation principles in the actuarial literature are the expected value principle and the variance principles. Denoting by C the insurance's loss, under the expected value principle (EVP) the premium is calculated by $\lambda = (1+\Theta)\mathbb{E}[C]$, for some safety loading $\Theta > 0$. While under the variance principle (VP) the premium is $\lambda = \mathbb{E}[C] + \Gamma \cdot \text{Var}\,(C)$, for some $\Gamma > 0$.

The company's reserve process over time can be described as a stochastic process in which two cash flows, incoming premiums and outgoing claims:

$$R_t = R_0 + \lambda_t - C_t$$

where C_t and λ_t are cumulative losses and premia over $[0, t]$, respectively, and $R_0 > 0$ is the initial capital. Under the EVP and VP premia principles the reserve process satisfies the so-called *net profit condition* that is $\mathbb{E}[C_t] < \mathbb{E}[\lambda_t]$ or equivalently $\mathbb{E}[R_t] > R_0$ for any time $t > 0$. This condition can be interpreted as the average income strictly larger than the average outflow. For classical models, such as the Cramér–Lundberg model where the claim arrival intensity is assumed constant, the *net profit condition* implies that there is a positive probability for the company not to fail (see Grandell, 1991).

As we can see in our empirical analysis (see Section 1) frequency and severity of natural catastrophes have high variability and classical models are not suitable to describe such events. If we price premiums according to the classical premium principles (EVP, VP), but not with respect to how big fluctuations we can have, it could have major consequences in the most extreme cases.

As demonstrated in our empirical analysis, the frequency and severity of natural disasters have a high variability and classical models are ill suited for describing such events. Thus, an evaluation based on the classical premium principles (EVP, VP), which does not take into account large fluctuations, could have important consequences in case of extreme events. For this reason, the results shown could help insurance companies to manage their risks in the face of claims due to natural disasters by providing an estimation of the maximal loss at 99%. Precisely, we have proved that log-cumulative losses are lower than $x_t^F + \sigma_t^F + Z_t$ with probability 99% (e.g. see Fig. 4), hence apply the following cumulative premia

$$\lambda_t = \prod_{s=1}^{s=t} e^{x^{F_s} + \sigma^{F_s} + Z_s}$$

implies that $\mathbb{P}(R_t > R_0) = 0.99$ for any time $t > 0$.

6. Conclusions

This work introduces an innovative model for predicting the expected value of losses resulting from natural disasters and their volatility over the course of 1, 5, 10, and 15 years. The proposed model is based on a generalized two-factor square-root approach, which incorporates stochastic correlation via a Brownian motion to link losses with volatility. The model we developed is a generalized two-factor square-root model that links losses with volatility through stochastic correlation following a Brownian motion. However, it is worth noting that while generalized linear models are widely used in the pricing of non-life insurance contracts (Laudagé, Desmettre, & Wenzel, 2019), they are not suitable for extreme claims. Therefore, to determine the maximum loss that could occur in terms of Value at Risk (VaR), we utilized the Generalized Pareto Distribution (GPD). The accuracy of our model was then compared with four baseline models, including AR, G2++, EVM, and GLM. We evaluated the model's performance by backtesting exceedances over the forecasted VaR, which serves as the upper bound of the GPD. Our model performed favorably compared to the benchmarks in terms of forecasting efficiency and backtests provided further validation of the chosen VaR.

The study, responding to deficiencies in Catastrophe Bond Pricing Models (CBPM) highlighted by Anggraeni et al. (2022), addresses challenges related to GEV, trigger model intricacies, ARIMA limitations, and CIR inefficacy. Using a Generalized Pareto Distribution (GPD), the approach estimates maximum potential losses (VaR) for different natural disasters. The insights stress the importance of mitigating moral hazard for investors near the trigger. The market demands an accurate and transparent earthquake catastrophe bond pricing model (Götze & Gürtler, 2020; Gürtler et al., 2016; Kiohos & Paspati, 2021). Thus, this methodology applies as well to dramatic changes in a given line of business (LOB) due to unexpected events such as COVID-19 (Babuna et al., 2020; Farooq et al., 2021; Guerrero et al., 2023) and could be used for estimating the related insurance premia.

CRediT authorship contribution statement

Michele Bufalo: Conceptualization, Data curation, Formal analysis, Investigation, Methodology, Resources, Software, Supervision, Validation, Visualization, Writing – original draft, Writing – review & editing. **Claudia Ceci:** Conceptualization, Formal analysis, Investigation, Methodology, Supervision, Validation, Visualization, Writing – review & editing. **Giuseppe Orlando:** Conceptualization, Data curation, Formal analysis, Funding acquisition, Investigation, Methodology, Project administration, Resources, Supervision, Validation, Visualization, Writing – original draft, Writing – review & editing.

Declaration of competing interest

The authors declare that they have no known competing financial interests or personal relationships that could have appeared to influence the work reported in this paper.

Data availability

Our dataset is sourced from the Emergency Events Database (EM-DAT) hosted at the Centre for Research on the Epidemiology of Disasters (CRED).

Acknowledgements

The authors are members of INdAM (Istituto Nazionale di Alta Matematica of Italy) GNAMPA (Gruppo Nazionale per l'Analisi Matematica, la Probabilità e le loro Applicazioni). C.C. has been partially supported through Project U-UFMBAZ-2020-000791. M.B. acknowledges support from GNAMPA for researching on anomalous diffusion and its applications to fractal domains: Physics and Mathematical Finance. G.O. acknowledges support from the Spanish Ministry of Science and Innovation (PID2022-138144NB-I00), the Center for Market Studies and Spatial Economics at the HSE University, and GNAMPA for researching on anomalous diffusion and its applications to fractal domains: Physics and Mathematical Finance. The authors thank the anonymous reviewers for their valuable feedback.

Appendix. Graphical and statistical evidences

In this section, we report some figures showing the out-of-sample results we obtained with our model. For each type of natural disaster first, we show the expected loss alongside the upper bound of our estimate (i.e. a sort of forecasted worst case). Then, as the insurer needs to keep under control the volatility of the losses, we also display the pointwise volatility. See Figs. A.8, A.11, A.14, A.17. After that we show the variation of z_t and, finally, the forecasts with different time horizons (5, 10 and 15 years) jointly with their related upper bounds. The latter with the usual intent to keep the exceedances under control. See Figs. A.9, A.10, A.12, A.13, A.15, A.16, A.18, A.19. Tables A.11, A.12, A.13, A.14 show parameters estimations and their confidence intervals for all studied natural disasters. As documented, both figures and tables support the validity of the proposed model.

A.1. Storm

Expected loss for storm alongside the upper bound of our estimate, representing a forecasted worst-case scenario and pointwise volatility for different time horizons (5, 10, and 15 years) along with their corresponding upper bounds, aimed at controlling exceedances. See Figs. A.8–A.10 and Table A.11 for the parameter estimation presented in the table.

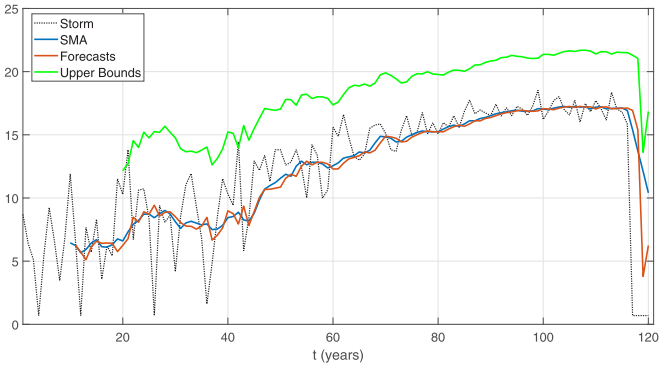

(a) Storm Forecasts. The (dotted) black line is the log-losses of the natural disaster X_t, the blue line is its SMA (ex post), the red line represents the corresponding forecasts x_t^F; finally the green line refers to the upper bound VaR_{GPD} computed as $x_t^F + \sigma_t^F + Z_t$ with $L' = 119$. Out of sample forecasts.

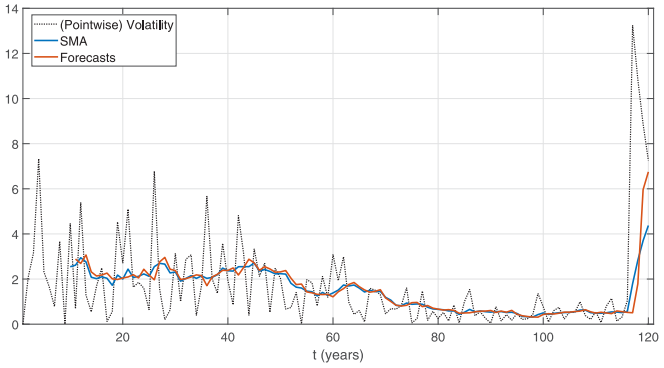

(b) Storm volatility Forecasts. The black (dotted) line is the (pointwise) volatility of the log-losses of disaster V_t, the blue line is its SMA (ex post), the red line represents the corresponding forecasts σ_t^F.

Fig. A.8. Storm and its (pointwise) volatility forecasts.

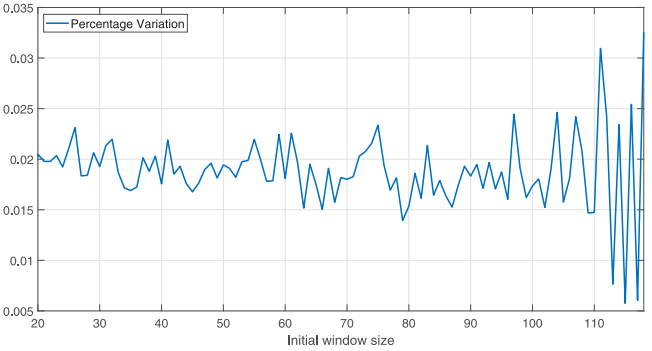

Fig. A.9. Percentage variation of Z_t for different initial window size $L' \geq 20$, for any $t \geq L'$.

Table A.11
Storm simulations. Parameters estimations and their confidence intervals.

Parameter	Estimation	Confidence interval
δ	8.8932	[6.5401, 11.2462]
γ	2.5350	[2.0964, 2.9737]
η	7.0072	[6.1519 7.8626]
k	0.9975	[0.9150, 1.0801]
θ	11.2355	[10.4381, 12.0330]
α	5.3503	[4.6972, 6.0034]

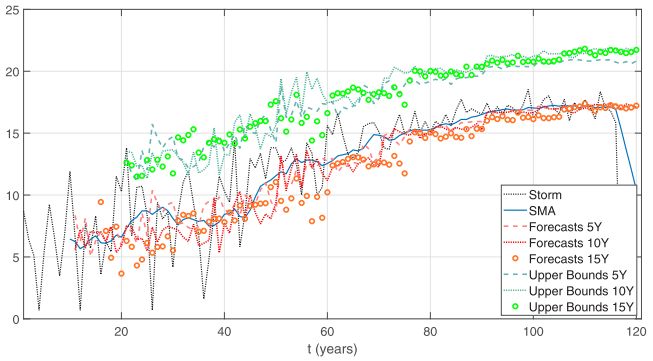

Fig. A.10. Storm log-losses forecasts for the next 5, 10 and 15 years.

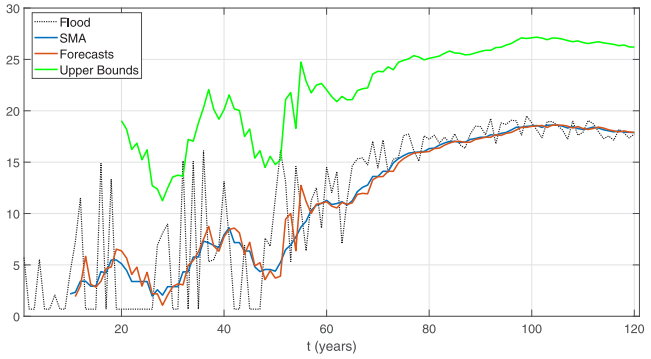

(a) Flood Forecasts. The (dotted) black line is the log-losses of the natural disaster X_t, the blue line is its SMA (ex post), the red line represents the corresponding forecasts x_t^F; finally the green line refers to the upper bound VaR_{GPD} computed as $x_t^F + \sigma_t^F + Z_t$ with $L' = 119$. Out of sample forecasts.

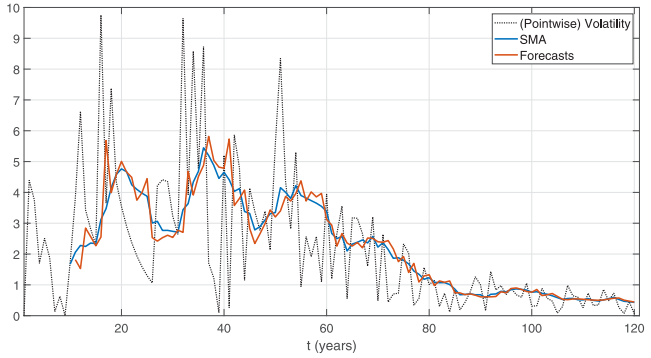

(b) Flood volatility Forecasts. The black (dotted) line is the (pointwise) volatility of the log-losses of disaster V_t, the blue line is its SMA (ex post), the red line represents the corresponding forecasts σ_t^F.

Fig. A.11. Flood and its (pointwise) volatility forecasts.

A.2. Flood

Expected loss for flood alongside the upper bound of our estimate, representing a forecasted worst-case scenario and pointwise volatility for different time horizons (5, 10, and 15 years) along with their corresponding upper bounds, aimed at controlling exceedances. See Figs. A.11–A.13 and Table A.12 for the parameter estimation presented in the table.

A.3. Drought

Expected loss for drought alongside the upper bound of our estimate, representing a forecasted worst-case scenario and pointwise volatility for different time horizons (5, 10, and 15 years) along with their corresponding upper bounds, aimed at controlling exceedances. See Figs. A.14–A.16 and Table A.13 for the parameter estimation presented in the table.

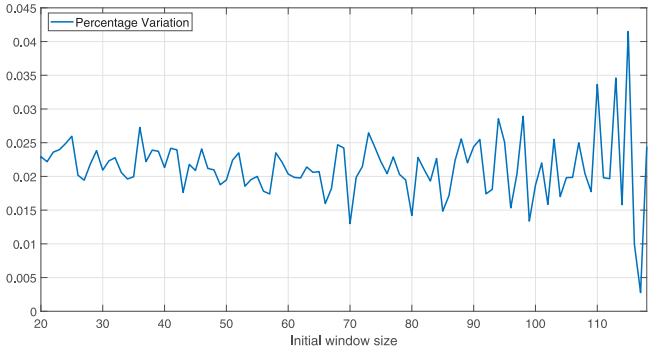

Fig. A.12. Percentage variation of Z_t for different initial window size $L' \geq 20$, for any $t \geq L'$.

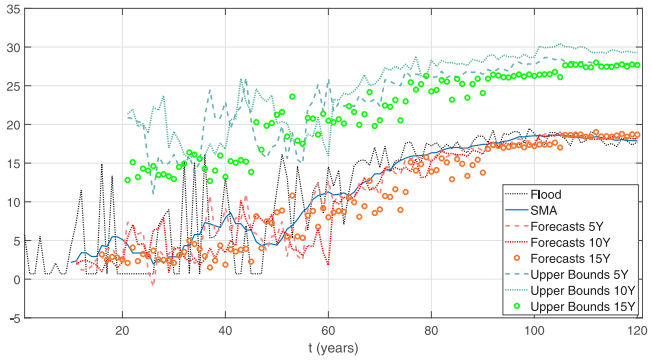

Fig. A.13. Flood log-losses forecasts for the next 5, 10 and 15 years.

Table A.12
Flood simulations. Parameters estimations and their confidence intervals.

Parameter	Estimation	Confidence interval
δ	18.2315	[14.3643, 22.0987]
γ	2.8611	[2.4349, 3.2872]
η	9.9978	[8.7774, 11.2182]
k	1.8312	[1.5891, 2.0733]
θ	11.8324	[10.5950, 13.0698]
α	9.5945	[8.4233, 10.7656]

Table A.13
Drought simulations. Parameters estimations and their confidence intervals.

Parameter	Estimation	Confidence interval
δ	4.7191	[3.7702, 5.6679]
γ	3.9016	[3.3422, 4.4611]
η	5.9423	[5.2170, 6.6677]
k	2.0527	[1.6437, 2.4617]
θ	8.8766	[7.6118, 10.1413]
α	10.2872	[9.0314, 11.5429]

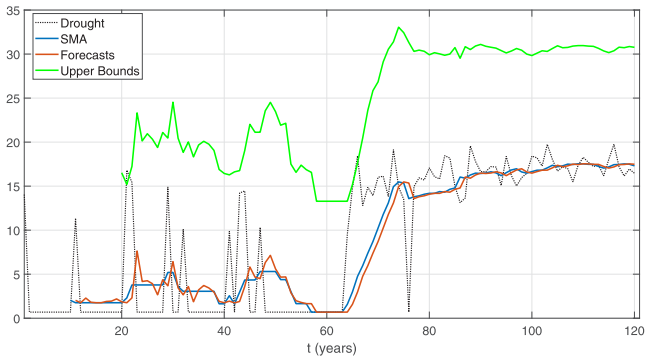

(a) Drought Forecasts. The (dotted) black line is the log-losses of the natural disaster X_t, the blue line is its SMA (ex post), the red line represents the corresponding forecasts x_t^F; finally the green line refers to the upper bound VaR_{GPD} computed as $x_t^F + \sigma_t^F + Z_t$ with $L' = 119$. Out of sample forecasts.

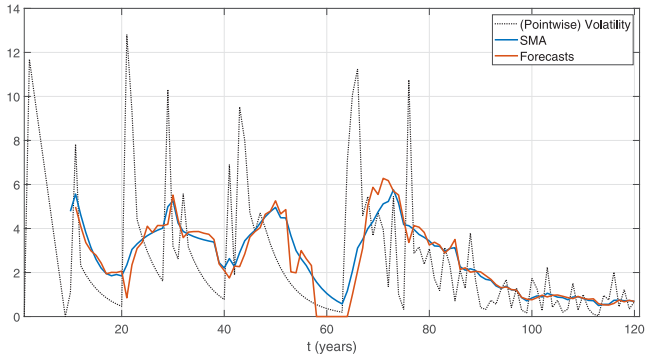

(b) Drought volatility Forecasts. The black (dotted) line is the (pointwise) volatility of the log-losses of disaster V_t, the blue line is its SMA (ex post), the red line represents the corresponding forecasts σ_t^F.

Fig. A.14. Drought and its (pointwise) volatility forecasts.

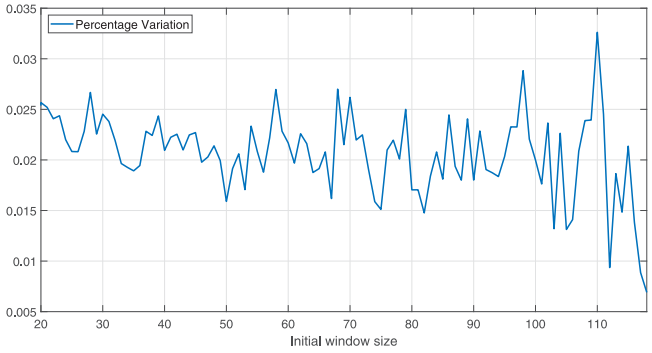

Fig. A.15. Percentage variation of Z_t for different initial window size $L' \geq 20$, for any $t \geq L'$.

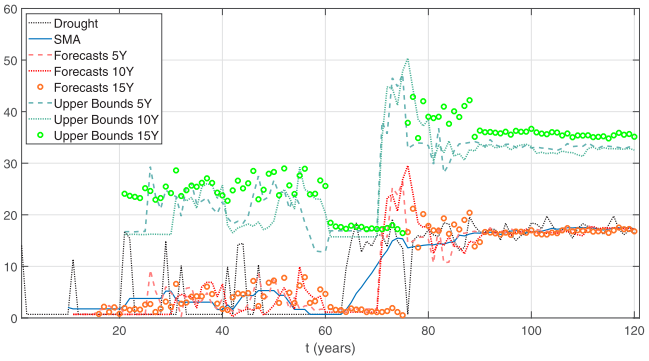

Fig. A.16. Drought log-losses forecasts for the next 5, 10 and 15 years.

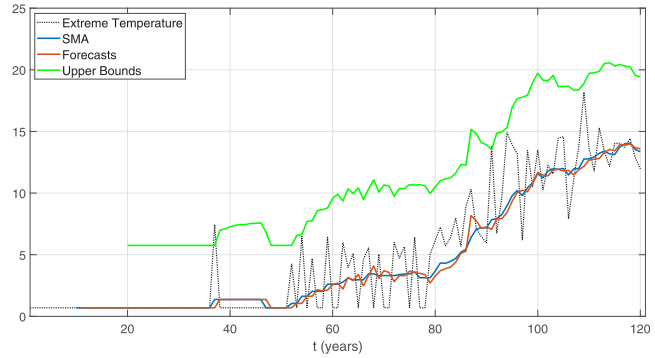

(a) Extreme temperature Forecasts. The (dotted) black line is the log-losses of the natural disaster X_t, the blue line is its SMA (ex post), the red line represents the corresponding forecasts x_t^F; finally the green line refers to the upper bound VaR_{GPD} computed as $x_t^F + \sigma_t^F + Z_t$ with $L' = 119$. Out of sample forecasts.

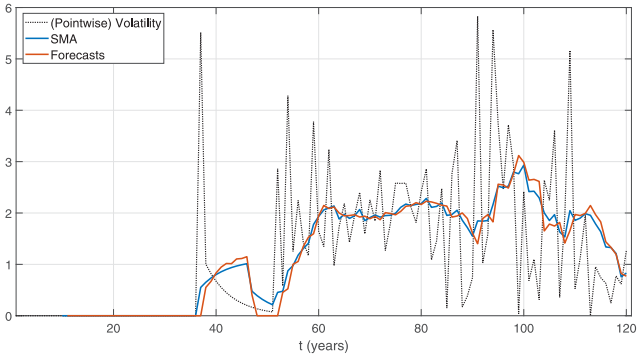

(b) Extreme temperature volatility Forecasts. The black (dotted) line is the (pointwise) volatility of the log-losses of disaster V_t, the blue line is its SMA (ex post), the red line represents the corresponding forecasts σ_t^F.

Fig. A.17. Extreme temperature and its (pointwise) volatility forecasts.

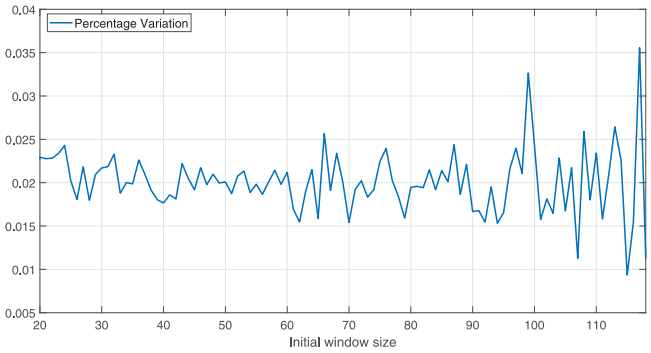

Fig. A.18. Percentage variation of Z_t for different initial window size $L' \geq 20$, for any $t \geq L'$.

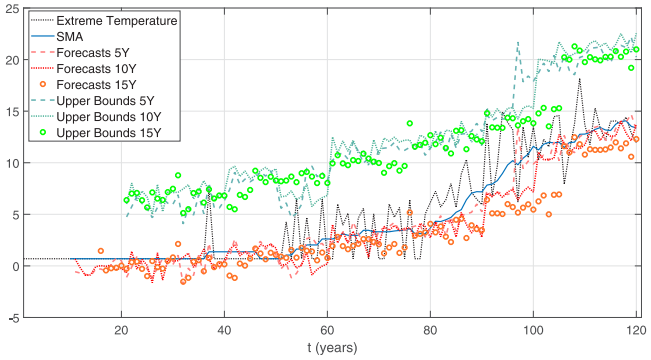

Fig. A.19. Extreme Temperature log-losses forecasts for the next 5, 10 and 15 years.

Table A.14
Extreme temperature simulations. Parameters estimations and their confidence intervals.

Parameter	Estimation	Confidence interval
δ	3.0007	[2.2068, 3.7947]
γ	1.6104	[1.3318, 1.8891]
η	5.3839	[4.7267, 6.0411]
k	2.3014	[1.6742, 2.9285]
θ	5.0811	[4.1849, 5.9773]
α	7.6339	[6.7020, 8.5657]

A.4. Extreme temperature

Expected loss for extreme temperature alongside the upper bound of our estimate, representing a forecasted worst-case scenario and pointwise volatility for different time horizons (5, 10, and 15 years) along with their corresponding upper bounds, aimed at controlling exceedances. See Figs. A.17–A.19 and Table A.14 for the parameter estimation presented in the table.

References

Acar, S., & Natcheva-Acar, K. (2009). *A guide on the implementation of the Heath-Jarrow-Morton two-factor Gaussian short rate model (HJM-G2++)*: *Berichte des Fraunhofer-Instituts für Techno- und Wirtschaftsmathematik (ITWM Report)*, (170), Fraunhofer (ITWM).

Ahlip, R., Park, L. A., & Prodan, A. (2017). Pricing currency options in the Heston/CIR double exponential jump-diffusion model. *International Journal of Financial Engineering*, *4*(01), Article 1750013.

Alvarez-Ramirez, J., Alvarez, J., Rodriguez, E., & Fernandez-Anaya, G. (2008). Time-varying Hurst exponent for US stock markets. *Physica A: Statistical Mechanics and Its Applications*, *387*(24), 6159–6169.

Anggraeni, W., Supian, S., Sukono, & Halim, N. B. A. (2022). Earthquake catastrophe bond pricing using extreme value theory: A mini-review approach. *Mathematics*, *10*(22), 4196.

Ascione, G., Bufalo, M., & Orlando, G. (2024). Modeling volatility of disaster-affected populations: A non-homogeneous geometric-skew Brownian motion approach. *Communications in Nonlinear Science and Numerical Simulation*, *130*, Article 107761.

Babuna, P., Yang, X., Gyilbag, A., Awudi, D. A., Ngmenbelle, D., & Bian, D. (2020). The Impact of COVID-19 on the Insurance Industry. *International Journal of Environmental Research and Public Health*, [ISSN: 1660-4601] *17*(16), 5766. http://dx.doi.org/10.3390/ijerph17165766.

Bacry, E., Mastromatteo, I., & Muzy, J.-F. (2015). Hawkes processes in finance. *Market Microstructure and Liquidity*, *1*(01), Article 1550005.
Balthazar, L. (2006). The regulation of market risk: The 1996 amendment. In *From basel 1 to basel 3: the integration of state-of-the-art risk modeling in banking regulation* (pp. 23–31). Springer.
Basel Committee (1996). *Supervisory framework for the use of backtesting in conjunction with the internal models approach to market risk capital requirements*. Switzerland: Basel Committee on Banking and Supervision.
Benali, N., & Feki, R. (2017). The impact of natural disasters on insurers' profitability: Evidence from Property/Casualty Insurance company in United States. *Research in International Business and Finance*, *42*, 1394–1400.
Bollerslev, T. (1986). Generalized autoregressive conditional heteroskedasticity. *Journal of Econometrics*, *31*(3), 307–327.
Born, P., & Viscusi, W. K. (2006). The catastrophic effects of natural disasters on insurance markets. *Journal of Risk and Uncertainty*, *33*(1), 55–72.
Brigo, D., & Mercurio, F. (2006). *Interest rate models-theory and practice: with smile, inflation and credit*. Berlin, Heidelberg: Springer-Verlag.
Cai, J.-J., Wan, P., & Ozel, G. (2020). Parametric and non-parametric estimation of extreme earthquake event: the joint tail inference for mainshocks and aftershocks. *Extremes*, 1–16.
Calder, A., Couper, A., Lo, J., & Aspen, P. (2012). Catastrophe model blending techniques and governance. The Acturial Profession.
Carbone, A., Castelli, G., & Stanley, H. E. (2004). Time-dependent hurst exponent in financial time series. *Physica A. Statistical Mechanics and its Applications*, *344*(1–2), 267–271.
Chavas, D., Yonekura, E., Karamperidou, C., Cavanaugh, N., & Serafin, K. (2013). US hurricanes and economic damage: Extreme value perspective. *Natural Hazards Review*, *14*(4), 237–246.
Chen, J., Lei, X., Zhang, L., & Peng, B. (2015). Using extreme value theory approaches to forecast the probability of outbreak of highly pathogenic influenza in Zhejiang, China. *PLoS One*, *10*(2), Article e0118521.
Christoffersen, P. F. (1998). Evaluating interval forecasts. *International Economic Review*, 841–862.
Christoffersen, P., Heston, S., & Jacobs, K. (2009). The shape and term structure of the index option smirk: Why multifactor stochastic volatility models work so well. *Management Science*, *55*(12), 1914–1932.
Coles, S., Bawa, J., Trenner, L., & Dorazio, P. (2001). *Vol. 208*, *An introduction to statistical modeling of extreme values*. Springer.
Cox, S. H., Lin, Y., & Pedersen, H. (2010). Mortality risk modeling: Applications to insurance securitization. *Insurance: Mathematics & Economics*, *46*(1), 242–253.
CRED (2020). CRED's emergency events database (EM-DAT). URL https://www.emdat.be/. (Accessed 03 January 2020).
De Jong, P., & Heller, G. Z. (2008). *Generalized linear models for insurance data*. Cambridge University Press.
Eichler, M., Dahlhaus, R., & Dueck, J. (2017). Graphical modeling for multivariate hawkes processes with nonparametric link functions. *Journal of Time Series Analysis*, *38*(2), 225–242.
Embrechts, P., Liniger, T., & Lin, L. (2011). Multivariate Hawkes processes: an application to financial data. *Journal of Applied Probability*, *48*(A), 367–378.
Ewald, C.-O., Zhang, A., & Zong, Z. (2019). On the calibration of the Schwartz two-factor model to WTI crude oil options and the extended Kalman filter. *Annals of Operations Research*, *282*(1–2), 119–130.
Faff, R., & Treepongkaruna, S. (2013). A re-examination of the empirical performance of the longstaff and schwartz two-factor term structure model using real yield data. *Australian Journal of Management*, *38*(2), 333–352.
Farooq, U., Nasir, A., Bilal, & Quddoos, M. U. (2021). The impact of COVID-19 pandemic on abnormal returns of insurance firms: a cross-country evidence. *Applied Economics*, [ISSN: 0003-6846] http://dx.doi.org/10.1080/00036846.2021.1884839.
Goldburd, M., Khare, A., & Tevet, D. (2016). *CAS monographs series*, *Generalized linear models for insurance rating*. (5), Casualty Actuarial Society.
Götze, T., & Gürtler, M. (2020). Risk transfer and moral hazard: An examination on the market for insurance-linked securities. *Journal of Economic Behaviour and Organization*, *180*, 758–777.
Grandell, J. (1991). *Aspects of risk theory*. New York: Springer-Verlag.
Guerrero, J., del Carmen Galiano, M., & Orlando, G. (2023). Modeling COVID-19 pandemic with financial markets models: The case of Jaén (Spain). *Mathematical Biosciences and Engineering*, *20*(5), 9080–9100.
Gürtler, M., Hibbeln, M., & Winkelvos, C. (2016). The impact of the financial crisis and natural catastrophes on CAT bonds. *The Journal of Risk and Insurance*, *83*(3), 579–612.
Hall, E. C., & Willett, R. M. (2016). Tracking dynamic point processes on networks. *Institute of Electrical and Electronics Engineers. Transactions on Information Theory*, *62*(7), 4327–4346.
Hanafy, M., et al. (2020). Application of generalized Pareto in non-life insurance. *Journal of Financial Risk Management*, *9*(03), 334.
Hawkes, A. G. (2018). Hawkes processes and their applications to finance: a review. *Quantitative Finance*, *18*(2), 193–198.
Heston, S. L. (1993). A closed-form solution for options with stochastic volatility with applications to bond and currency options. *The Review of Financial Studies*, *6*(2), 327–343.
Holland, P. W., & Welsch, R. E. (1977). Robust regression using iteratively reweighted least-squares. *Communications in Statistics-Theory and Methods*, *6*(9), 813–827.
Hsieh, P.-H. (2004). A data-analytic method for forecasting next record catastrophe loss. *Journal of Risk and Insurance*, *71*(2), 309–322.
Hull, J. C., & White, A. D. (1994). Numerical procedures for implementing term structure models II: two-factor models. *The Journal of Derivatives*, *2*(2), 37–48.
Hurst, H. E. (1956). Methods of using long-term storage in reservoirs. *Proceedings of the Institution of Civil Engineers*, *5*(5), 519–543.
Jeanblanc, M., Yor, M., & Chesney, M. (2009). Mathematical methods for financial markets. In *Springer finance*, London: Springer-Verlag.
Jin, J.-L., Cheng, J., & Wei, Y.-M. (2008). Forecasting flood disasters using an accelerated genetic algorithm: Examples of two case studies for China. *Natural Hazards*, *44*(1), 85–92.
Jorion, P., et al. (2009). *Vol. 406*, *Financial risk manager handbook*. John Wiley & Sons.
Kiohos, A., & Paspati, M. (2021). Alternative to Insurance Risk Transfer: Creating a catastrophe bond for Romanian earthquakes. *Bulletin of Applied Economics*, *8*(1), 1.
Kladıvko, K. (2007). Maximum likelihood estimation of the Cox-Ingersoll-Ross process: the Matlab implementation. *Technical Computing Prague*.
Kohrs, H., Mühlichen, H., Auer, B. R., & Schuhmacher, F. (2019). Pricing and risk of swing contracts in natural gas markets. *Review of Derivatives Research*, *22*(1), 77–167.
Kupiec, P. (1995). Techniques for verifying the accuracy of risk measurement models. *The Journal of Derivatives*, *3*(2).
Laudagé, C., Desmettre, S., & Wenzel, J. (2019). Severity modeling of extreme insurance claims for tariffication. *Insurance: Mathematics & Economics*, *88*, 77–92.
Longstaff, F. A., & Schwartz, E. S. (1992). Interest rate volatility and the term structure: A two-factor general equilibrium model. *The Journal of Finance*, *47*(4), 1259–1282.
Lythe, R., Shah, L., & Grossi, P. (2008). A guide to catastrophe modelling. *The Review*.
Mandelbrot, B. B., & Van Ness, J. W. (1968). Fractional Brownian motions, fractional noises and applications. *SIAM Review*, *10*(4), 422–437.
Mandelbrot, B. B., & Wallis, J. R. (1969). Robustness of the rescaled range R/S in the measurement of noncyclic long run statistical dependence. *Water Resources Research*, *5*(5), 967–988.
Martins, A. L. A., Liska, G. R., Beijo, L. A., de Menezes, F. S., & Cirillo, M. Â. (2020). Generalized Pareto distribution applied to the analysis of maximum rainfall events in Uruguaiana, RS, Brazil. *SN Applied Sciences*, *2*(9), 1–13.
Mitchell-Wallace, K., Jones, M., Hillier, J., & Foote, M. (2017). *Natural catastrophe risk management and modelling: A practitioner's guide*. John Wiley & Sons.
Morton, M., & Levy, J. L. (2011). Challenges in disaster data collection during recent disasters. *Prehospital and Disaster Medicine*, *26*(3), 196–201.

Nawrocki, D. (1995). R/S analysis and long term dependence in stock market indices. *Managerial Finance*, *21*, 78.
Nelder, J. A., & Wedderburn, R. W. (1972). Generalized linear models. *Journal of the Royal Statistical Society: Series A (General)*, *135*(3), 370–384.
Ogata, Y. (1988). Statistical models for earthquake occurrences and residual analysis for point processes. *Journal of the American Statistical Association*, *83*(401), 9–27.
Ohlsson, E., & Johansson, B. (2010). *Vol. 174, Non-life insurance pricing with generalized linear models*. Springer.
Orlando, G., & Bufalo, M. (2021). Interest rates forecasting: Between Hull and White and the CIR#—How to make a single-factor model work. *Journal of Forecasting*, [ISSN: 0277-6693] *40*(8), 1566–1580. http://dx.doi.org/10.1002/for.2783.
Orlando, G., & Bufalo, M. (2022). A generalized two-factor square-root framework for modeling occurrences of natural catastrophes. *Journal of Forecasting*, [ISSN: 0277-6693] *41*(8), 1608–1622. http://dx.doi.org/10.1002/for.2880.
Orlando, G., & Bufalo, M. (2023). Time series forecasting with the CIR# model: from hectic markets sentiments to regular seasonal tourism. *Technological and Economic Development of Economy*, [ISSN: 2029-4921] *29*(4), 1216–1238. http://dx.doi.org/10.3846/tede.2023.19294.
Orlando, G., Mininni, R. M., & Bufalo, M. (2018). A new approach to CIR short-term rates modelling. In M. Mili, R. Medina Samaniego, & d. P. Filippo (Eds.), *New methods in fixed income modeling - fixed income modeling* (pp. 35–44). Springer International (USA).
Orlando, G., Mininni, R. M., & Bufalo, M. (2019a). A new approach to forecast market interest rates through the CIR model. *Studies in Economics and Finance*.
Orlando, G., Mininni, R. M., & Bufalo, M. (2019b). Forecasting interest rates through Vasicek and CIR models: a partitioning approach. *Journal of Forecasting*.
Orlando, G., Mininni, R. M., & Bufalo, M. (2019c). Interest rates calibration with a CIR model. *The Journal of Risk Finance*.
Pickands III, J. (1975). Statistical inference using extreme order statistics. *The Annals of Statistics*, *3*(1), 119–131.
Povinelli, R. J. (2000). Identifying temporal patterns for characterization and prediction of financial time series events. In *International workshop on temporal, spatial, and spatio-temporal data mining* (pp. 46–61). Springer.
Qian, B., & Rasheed, K. (2004). Hurst exponent and financial market predictability. In *IASTED conference on financial engineering and applications* (pp. 203–209).
Recchioni, M. C., & Sun, Y. (2016). An explicitly solvable Heston model with stochastic interest rate. *European Journal of Operational Research*, *249*(1), 359–377.
Rouah, F. D. (2013). *The Heston model and its extensions in matlab and C*. John Wiley & Sons.
Rypdal, M., & Løvsletten, O. (2013). Modeling electricity spot prices using mean-reverting multifractal processes. *Physica A. Statistical Mechanics and its Applications*, *392*(1), 194–207.
Shang, J., & Sun, M. (2019). Geometric Hawkes processes with graph convolutional recurrent neural networks. *Vol. 33*, In *Proceedings of the AAAI conference on artificial intelligence* (pp. 4878–4885).
Shreve, S. E. (2004). *Vol. 11, Stochastic calculus for finance II: Continuous-time models*. Springer Science & Business Media.
Tsuchiya, O. (2019). Two-factor hull-white model revisited: correlation structure for two-factor interest rate model in CVA calculation. Available at SSRN 3338987.
Utsu, T. (1970). Aftershocks and earthquake statistics (I): Some parameters which characterize an aftershock sequence and their interrelations. *Journal of the Faculty of Science, Series 7, Geophysics*, *3*(3), 129–195.
Vyushin, D., Kushner, P., & Zwiers, F. (2012). Modeling and understanding persistence of climate variability. *Journal of Geophysical Research: Atmospheres*, *117*(D21).
Zivot, E. (2009). Practical issues in the analysis of univariate GARCH models. In *Handbook of financial time series* (pp. 113–155). Springer.